

Radiation enhancement and temperature in the collapse regime of gravitational scattering

Marcello Ciafaloni*

Dipartimento di Fisica, Universita' di Firenze, Via Sansone 1, 50019 Sesto Fiorentino, Italy

Dimitri Colferai†

Dipartimento di Fisica, Università di Firenze and INFN Firenze, Via Sansone 1, 50019 Sesto Fiorentino, Italy

(Received 20 January 2017; published 6 April 2017)

We generalize the semiclassical treatment of graviton radiation to gravitational scattering at very large energies $\sqrt{s} \gg m_p$ and finite scattering angles Θ_s , so as to approach the collapse regime of impact parameters $b \simeq b_c \sim R \equiv 2G\sqrt{s}$. Our basic tool is the extension of the recently proposed, unified form of radiation to the Amati Ciafaloni Veneziano (ACV) reduced-action model and to its resummed-eikonal exchange. By superimposing that radiation all over eikonal scattering, we are able to derive the corresponding (unitary) coherent-state operator. The resulting graviton spectrum, tuned on the gravitational radius R , fully agrees with previous calculations for small angles $\Theta_s \ll 1$ but, for sizeable angles $\Theta_s(b) \leq \Theta_c = \mathcal{O}(1)$, acquires an exponential cutoff of the large ωR region, due to energy conservation, so as to emit a finite fraction of the total energy. In the approach-to-collapse regime of $b \rightarrow b_c^+$, we find a radiation enhancement due to large tidal forces, so that the whole energy is radiated off, with a large multiplicity $\langle N \rangle \sim Gs \gg 1$ and a well-defined frequency cutoff of order R^{-1} . The latter corresponds to the Hawking temperature for a black hole of mass notably smaller than \sqrt{s} .

DOI: 10.1103/PhysRevD.95.086003

I. INTRODUCTION

The investigation of trans-Planckian-energy gravitational scattering performed since the 1980s [1–8] and applied to the collapse regime [9–12] has been recently revived at both the classical [13] and quantum levels [14,15] with the purpose of describing the radiation associated to extreme energies and of gaining a better understanding of a possibly collapsing system. A bridge between the different approaches of Refs. [14,15] has also been devised [16].

Here, we follow essentially the ACV path [5,7–9], that is mostly an effective theory based on s -channel iteration (eikonal scattering) and motivated by the smallness of fixed-angle amplitudes in string gravity [4] and by the high-energy dominance of the spin-2 graviton exchange, at small momentum transfers [1–3]. In fact, a key feature of eikonal scattering is that the large momentum transfers built up at a fixed scattering angle (e.g. the Einstein deflection angle $\Theta_E \equiv 2R/b$)— $R \equiv 2G\sqrt{s}$ being the gravitational radius—is due to a large number $\langle n \rangle = Gs/\hbar \equiv \alpha_G \gg 1$ of single hits with very small scattering angle $\theta_m \sim \hbar/bE$. By following these lines, ACV [8] proposed an all-order generalization of the semiclassical approach based on an effective action [6,17], that allows one in principle to compute corrections to the eikonal functions depending on

the expansion parameter R^2/b^2 [by neglecting, in string gravity, the smaller ones $\mathcal{O}(l_s^2/b^2)$ [5,18] if $l_p < l_s \ll R$]. In its axisymmetric formulation, the eikonal resummation reduces to a solvable model in one-dimensional radial space, that was worked out explicitly in Ref. [9]. Such a reduced-action model allows one to treat sizeable angles R/b , up to a singularity point $b_c = \sqrt{3\sqrt{3}/2}R$ where a branch point of critical index $3/2$ occurs in the action, as signal of a possible classical collapse.

The main purpose of the present paper is to extend the radiation treatment of Refs. [15,19] to larger angles, by applying it to the ACV-resummed eikonal, in order to achieve comparable progress at the radiation level. We shall then use it to study the extreme energy regime of a possible classical collapse $b \rightarrow b_c^+ \sim R$.

Let us recall that the main qualitative understanding of Ref. [15], compared to previous approaches, was to disentangle the role of the gravitational radius R in the radiation process. In fact, by superimposing the radiation amplitudes associated to the various eikonal exchanges and by combining the large number $\langle n \rangle \sim \alpha_G = ER$ of emitters with the relatively small energy fraction $\hbar\omega/E$, Ciafaloni Colferai Veneziano (CCV) found that the relevant variable becomes ωR , which is thus needed to describe the interference pattern of the whole amplitude (Sec. II). In the present paper, we follow the same strategy, by replacing the leading eikonal (single-graviton exchange) by the resummed one (Sec. III).

*ciafaloni@fi.infn.it

†colferai@fi.infn.it

There is, however, an important technical point to be understood. The single-exchange radiation amplitude was determined in Refs. [15,19] by unifying in the $E \gg \hbar\omega$ regime the Regge region of large emission angles with the soft one. Such a unifying relationship involves a simple rescaling $E \rightarrow \hbar\omega$ of the soft amplitude and is exact for single-graviton exchange. Here, we wish to generalize the soft-based representation so obtained to all subleading eikonal contributions. No real proof of that statement is available yet. Nevertheless, we shall argue in Sec. III that, starting from the H diagram [7], the dominant Regge contributions are confined to the deep fragmentation regions of the incoming particles, thus allowing the approximate use of the unifying relationship mentioned before and of the ensuing soft-based representation.

By entering the large-angle region, we meet the issue of energy conservation, also [20–23]. Indeed, the coherent radiation state obtained by the soft-based formulation treats the fast particles as sources and thus neglects, in a first instance, conservation constraints. By introducing them explicitly in Sec. IV, we keep neglecting correlations that we argue to be small (Sec. III D). However, the overall effect of energy conservation is quite important, in the large-angle region, because it introduces an exponential cutoff which—though preserving quantum coherence—plays a role similar to the temperature in a statistical ensemble.

The validity of the exponential behavior and its role in approaching collapse are carefully discussed in Sec. IV C. The final outcome is that the whole energy is radiated off in the approach-to-collapse regime, by fixing the analog of the Hawking temperature [24,25] for our energetic sample of (coherent) radiation.

II. GRAVITON RADIATION IN SMALL-ANGLE TRANS-PLANCKIAN SCATTERING

The approach to gravitational scattering and radiation advocated in Ref. [19] is based on a semiclassical approximation to the S -matrix of the form

$$S \simeq \exp \left\{ 2i\hat{\delta} \left(\alpha_G, \frac{R}{b}, a_\lambda(\vec{q}) \right) \right\}, \quad (2.1)$$

where the eikonal operator $\hat{\delta}$ is a function of the effective coupling $\alpha_G \equiv Gs/\hbar$ and of the angular variable R/b (where $R \equiv 2G\sqrt{s}$ is the gravitational radius and b is the impact parameter) and a functional of the graviton step operators $a_\lambda(\vec{q})$ with helicity λ and momentum \vec{q} .

The semiclassical form (2.1) was argued in Ref. [9] to be valid in the strong-gravity regime $\alpha_G \gg 1$ with $R \gg b \gg l_s > l_p$, where l_s is the string length and $l_p \equiv \sqrt{\hbar G}$ is the Planck length. This means that we are, to start with, in the trans-Planckian regime $\sqrt{s} \gg m_p = \hbar/l_p$ at small scattering angles $\Theta_s \simeq \Theta_E \equiv 2R/b$, where Θ_E is the Einstein deflection angle. Quantum corrections to (2.1)

will involve the parameter l_p^2/b^2 (and l_s^2/b^2 if working within string gravity) and will be partly considered later on.

The eikonal operator is then obtained by resumming an infinite series of effective diagrams which include virtual graviton exchanges and real graviton emissions, as will be shortly reviewed in the following. In the small-angle and low-density limit, it is composed by two terms: (i) a c-number phase shift δ_0 generated by graviton exchanges between the external particles undergoing the scattering process and (ii) a linear superposition of creation and destruction operators which is responsible for graviton bremsstrahlung and associated quantum virtual corrections,

$$\begin{aligned} \hat{\delta} \left(\alpha_G, \frac{R}{b}, a_\lambda(\vec{q}) \right) &= \delta_0(b) + \int \frac{d^3q}{\hbar^3 \sqrt{2\omega}} \\ &\times \sum_{\lambda=\pm 2} [\mathfrak{M}_\lambda(\mathbf{b}, \vec{q}) a_\lambda^\dagger(\vec{q}) + \text{H.c.}] \\ &+ \mathcal{O}(a_\lambda^2), \end{aligned} \quad (2.2)$$

where higher powers of a_λ provide high-density corrections. This structure, which is valid for large impact parameters, i.e., for small values of the ratio $R/b \ll 1$, provides a unitary S -matrix describing the Einstein deflection of the scattered particles as well as its associated graviton radiation and its metric fields [9,26] and time delays [27].

Actually, the subject of this paper is to extend the above picture to smaller impact parameters $b \sim R$ where the gravitational interaction becomes really strong and a gravitational collapse is expected on classical grounds. We will show that, decreasing the impact parameter b up to some critical parameter $b_c \sim R$ of the order of the gravitational radius R , the form of the S -matrix maintains the form (2.1), (2.2) with calculable corrections to both the phase shift δ_0 (Sec. III A) and to the emission amplitude \mathfrak{M} (Sec. III C). We shall then discuss in detail (Sec. IV) what happens in the limit $b \rightarrow b_c$ from above.

A. Eikonal scattering

ACV [7] have shown that the leading contributions to the high-energy elastic scattering amplitude $p_1 + p_2 \rightarrow p'_1 + p'_2$ come from the s -channel iteration of soft-graviton exchanges, which can be represented by effective ladder diagrams as in Fig. 1. The generic ladder is built by iteration [i.e., four-dimensional (4D) convolution] of the basic rung

$$\begin{aligned} \mathcal{R}_1(p_1, p_2, Q) &= iM_1(Q^2, s) 2\pi\delta_+((p_1 - Q)^2) \\ &\times 2\pi\delta_+((p_2 + Q)^2), \\ M_1(Q^2, s) &\equiv -\frac{8\pi Gs^2}{Q^2}, \end{aligned} \quad (2.3)$$

which embodies the on-shell conditions of the scattered particles and the Newton-like elastic scattering amplitude M_1 in momentum space. The on-shell conditions and the

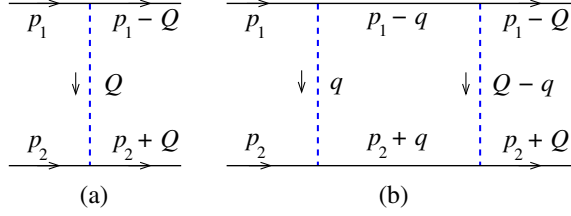


FIG. 1. (a) One- and (b) two-rung effective ladder diagrams determining the elastic S -matrix in the eikonal approximation. Solid lines: on-shell external particles; dashed lines: eikonal gravitational exchanges.

particular form of M_1 make it possible to express the n -rung amplitude as a 2D convolution in the form

$$\begin{aligned} iM_n(Q^2, s) &= \frac{i^n}{n!} \int \frac{d^2\mathbf{q}}{(2\pi)^2} M_{n-1}(-(\mathbf{Q}-\mathbf{q})^2, s) \frac{4\pi Gs}{q^2} \\ &= \frac{2s}{n!} \left[\otimes \frac{i4\pi Gs}{Q^2} \right], \end{aligned} \quad (2.4)$$

where boldface variables denote 2D Euclidean transverse components. By Fourier transforming from transverse momentum \mathbf{Q} to impact parameter \mathbf{b} , the full eikonal scattering amplitude can be diagonalized and exponentiated,

$$\frac{i}{2s} M(Q^2, s) \equiv \frac{i}{2s} \sum_{n=0}^{\infty} M_n(Q^2, s) = \int d^2\mathbf{b} e^{i\mathbf{Q}\cdot\mathbf{b}} e^{i2\delta_0(b,s)}, \quad (2.5)$$

in terms of the eikonal phase shift $\delta_0(b, s)$ defined as the Fourier transform of the single-exchange amplitude

$$\begin{aligned} 2\delta_0(b, s) &= \int \frac{d^2\mathbf{Q}}{(2\pi)^2} e^{-i\mathbf{Q}\cdot\mathbf{b}} \frac{4\pi Gs}{Q^2} \Theta(Q^2 - Q_0^2) \\ &= 2Gs \ln \frac{L}{b} + \mathcal{O}\left(\frac{b}{L}\right)^2, \end{aligned} \quad (2.6)$$

where $b \equiv |\mathbf{b}|$ and $L \equiv 2e^{-\gamma_E}/Q_0$ is a factorized—and thus irrelevant—infrared cutoff needed to regularize the “Coulomb” divergence typical of long-range interactions.

In order to go beyond the leading eikonal approximation, one has to consider other diagrams providing corrections of relative order $(R/b)^2$ to elastic scattering and also inelastic processes (graviton bremsstrahlung). The former will be dealt with in Sec. III; in the following in this section, we shall review graviton bremsstrahlung as derived in Ref. [19].

B. Unified emission amplitude from single-graviton exchange

In this subsection, we review the derivation of the unified emission amplitude for the basic process $2 \rightarrow 2 + \text{graviton}$. “Unified” means that such an amplitude is accurate for both

large (Regge region) and small (collinear region) graviton emission angles.

Consider the basic emission process $p_1 + p_2 \rightarrow p'_1 + p'_2 + q$ at tree level (Fig. 2) of a graviton of momentum $q^\mu: \mathbf{q} = \hbar\omega\boldsymbol{\theta}$ and helicity λ , assuming a relatively soft-emission energy $\hbar\omega \ll E$. Note that this restriction still allows for a huge graviton phase space, corresponding to classical frequencies potentially much larger than the characteristic scale R^{-1} , due to the large gravitational charge $\alpha_G \equiv Gs/\hbar \gg 1$.

We denote with \mathbf{q}_s the single-hit transverse momentum exchanged between particles 1 and 2, and with $\boldsymbol{\theta}_s = |\boldsymbol{\theta}_s|(\cos\phi_s, \sin\phi_s) = \mathbf{q}_s/E$, we denote the corresponding 2D scattering angle (including azimuth). For not too large emission angles $|\boldsymbol{\theta}| \ll (E/\hbar\omega)|\boldsymbol{\theta}_s|$, corresponding to $|\mathbf{q}| \ll |\mathbf{q}_s|$, Weinberg’s theorem expresses the emission amplitude as the product of the elastic amplitude M_1 and of the external-line insertion factor $J_W^{(\lambda)} \equiv J_W^{\mu\nu} \epsilon_{\mu\nu}^{(\lambda)*}$, where $\epsilon_{\mu\nu}^{(\lambda)}$ is the polarization tensor of the emitted graviton (see Ref. [19] for details) and $J_W^{\mu\nu}$ is the Weinberg current [28] [$\eta_i = +1(-1)$ for incoming (outgoing) lines]

$$\begin{aligned} J_W^{\mu\nu} &= \kappa \sum_i \eta_i \frac{p_i^\mu p_i^\nu}{p_i \cdot q} \\ &= \kappa \left(\frac{p_1^\mu p_1^\nu}{p_1 \cdot q} - \frac{p_1'^\mu p_1'^\nu}{p_1' \cdot q} + \frac{p_2^\mu p_2^\nu}{p_2 \cdot q} - \frac{p_2'^\mu p_2'^\nu}{p_2' \cdot q} \right). \end{aligned} \quad (2.7)$$

By referring, for definiteness, to the forward hemisphere and restricting ourselves to the forward region $|\boldsymbol{\theta}|, |\boldsymbol{\theta}_s| \ll 1$, one obtains the following explicit result [19] in the c.m. frame with $\mathbf{p}_1 = 0$,

$$J_W^{(\lambda)}(q^3 > 0; \boldsymbol{\theta}, \boldsymbol{\theta}_s) = \kappa \frac{E}{\hbar\omega} (e^{i\lambda(\phi_\theta - \phi_{\theta-s})} - 1), \quad (2.8)$$

leading to a factorized soft-emission amplitude

$$\begin{aligned} M_{\text{soft}}(\boldsymbol{\theta}_s, E, \boldsymbol{\theta}, \omega) &= M_{\text{el}}(E, \mathbf{Q}) J_W^{(\lambda)}\left(\frac{E}{\hbar\omega}, \boldsymbol{\theta}, \boldsymbol{\theta}_s\right) \\ &= \kappa^3 s^2 \frac{1}{E\hbar\omega\boldsymbol{\theta}_s^2} (e^{i\lambda(\phi_\theta - \phi_{\theta-s})} - 1). \end{aligned} \quad (2.9)$$

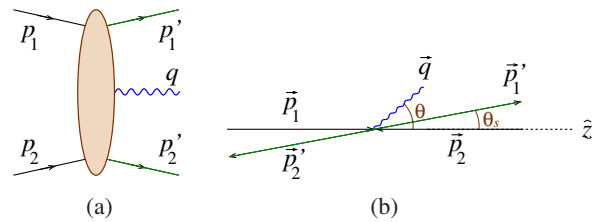


FIG. 2. (a) Diagram representing graviton emission (wavy line) in trans-Planckian scattering of two sources (straight lines). (b) Kinematics in the spatial momentum space.

The simple expression (2.8) shows a $1/\omega$ dependence, but no singularities at either $\theta = 0$ or $\theta = \theta_s$ as we might have expected from the $p_i \cdot q$ denominators occurring in (2.7). This is due to the helicity conservation zeros in the physical projections of the tensor numerators in (2.7).

The soft amplitude in impact parameter space is readily obtained by Fourier transforming with respect to $\mathbf{Q} = \mathbf{q}_s = E\boldsymbol{\theta}_s$ and reads

$$\begin{aligned} \mathcal{M}_{\text{soft}}^{(\lambda)}(\mathbf{b}, E, \boldsymbol{\theta}, \omega) &\equiv \frac{1}{(2\pi)^{3/2}} \frac{1}{4s} \int \frac{d^2\mathbf{q}_s}{(2\pi)^2} e^{i\mathbf{q}_s \cdot \mathbf{b}} M_{\text{soft}}(\mathbf{q}_s) \\ &= \sqrt{\alpha_G} \frac{R}{\pi} \int \frac{d^2\boldsymbol{\theta}_s}{2\pi\boldsymbol{\theta}_s^2} e^{i\frac{E}{\hbar}\mathbf{b} \cdot \boldsymbol{\theta}_s} \\ &\quad \times \frac{E}{\hbar\omega} \frac{1}{2} (e^{i\lambda(\phi_{\boldsymbol{\theta}} - \phi_{\boldsymbol{\theta}_s})} - 1) \\ &= \sqrt{\alpha_G} \frac{R}{\pi} e^{i\lambda\phi_{\boldsymbol{\theta}}} \int \frac{d^2\mathbf{z}}{2\pi|\mathbf{z}|^2 e^{i\lambda\phi_z}} \\ &\quad \times e^{i\mathbf{b}\omega\mathbf{z} \cdot \boldsymbol{\theta}} \frac{E}{\hbar\omega} \log \left| \hat{\mathbf{b}} - \frac{\hbar\omega}{E}\mathbf{z} \right|, \end{aligned} \quad (2.10)$$

where in the last line we have used an integral representation which will be very useful in the sequel.

For large emission angles $|\boldsymbol{\theta}| \gtrsim (E/\hbar\omega)|\boldsymbol{\theta}_s|$ such that $|\mathbf{q}| \gtrsim |\mathbf{q}_s|$, graviton emission from internal insertions is no longer negligible, and Weinberg's formula cannot be applied. However, this region of phase space is a subset of the so-called Regge region, characterized by emission angles $|\boldsymbol{\theta}| \gg |\boldsymbol{\theta}_s|$. In the Regge limit, the emission amplitude has a different factorized structure and a different emission current: Lipatov's current $J_L^{\mu\nu}$ [29]. Furthermore, one has to distinguish two transferred momenta $\mathbf{q}_{1(2)} \equiv \mathbf{p}_{1(2)} - \mathbf{p}'_{1(2)}$ such that $\mathbf{q} = \mathbf{q}_1 + \mathbf{q}_2$. In the c.m. frame with zero incidence angle ($\mathbf{p}_1 = E\boldsymbol{\Theta}_i = 0$) and in the forward region $|\boldsymbol{\theta}|, |\boldsymbol{\theta}_s| \ll 1$ (where we identify $\mathbf{q}_s = \mathbf{q}_2$), the helicity amplitude takes the form [19]

$$\begin{aligned} M_{\text{Regge}}^{(\lambda)}(\boldsymbol{\theta}_s, E, \boldsymbol{\theta}, \omega) &= \frac{\kappa^2 s^2}{|\mathbf{q}_1|^2 |\mathbf{q}_2|^2} J_L^{\mu\nu} \epsilon_{\mu\nu}^{(\lambda)*} \\ &= \kappa^3 s^2 \frac{1 - e^{i\lambda(\phi_{\mathbf{q}_2} - \phi_{\mathbf{q} - \mathbf{q}_2})}}{\mathbf{q}^2}, \end{aligned} \quad (2.11)$$

$$\begin{aligned} \mathcal{M}_{\text{Regge}}^{(\lambda)}(\mathbf{b}, E, \boldsymbol{\theta}, \omega) &= \sqrt{\alpha_G} \frac{R}{\pi} e^{i\lambda\phi_{\boldsymbol{\theta}}} \int \frac{d^2\mathbf{z}}{2\pi|\mathbf{z}|^2 e^{i\lambda\phi_z}} e^{i\mathbf{b}\omega\mathbf{z} \cdot \boldsymbol{\theta}} \\ &\quad \times (-\hat{\mathbf{b}} \cdot \mathbf{z} - \log |\hat{\mathbf{b}} - \mathbf{z}|). \end{aligned} \quad (2.12)$$

It is not difficult to verify that the soft and Regge amplitudes (2.9), (2.11) agree in the overlapping region of validity $|\boldsymbol{\theta}_s| \ll \boldsymbol{\theta} \ll (E/\hbar\omega)|\boldsymbol{\theta}_s|$. By exploiting the above expressions, we obtained a unifying amplitude that accurately describes both regimes and that can be written in terms of the soft amplitude only:

$$\begin{aligned} \frac{\mathcal{M}_{\text{matched}}^{(\lambda)}}{\sqrt{\alpha_G} \frac{R}{\pi} e^{i\lambda\phi_{\boldsymbol{\theta}}}} &= \int \frac{d^2\mathbf{z}}{2\pi|\mathbf{z}|^2 e^{i\lambda\phi_z}} e^{i\mathbf{b}\omega\mathbf{z} \cdot \boldsymbol{\theta}} \\ &\quad \times \left(\frac{E}{\hbar\omega} \log \left| \hat{\mathbf{b}} - \frac{\hbar\omega}{E}\mathbf{z} \right| - \log |\hat{\mathbf{b}} - \mathbf{z}| \right) \\ &= \text{soft}|_E - \text{soft}|_{\hbar\omega}. \end{aligned} \quad (2.13)$$

The result (2.13) is expressed in terms of the (ω -dependent) ‘‘soft’’ field¹

$$\begin{aligned} h_s^{(\lambda)}(\omega, \mathbf{z}) &\equiv \frac{1}{\pi^2 |\mathbf{z}|^2 e^{i\lambda\phi_z}} \left(\frac{E}{\hbar\omega} \log \left| \hat{\mathbf{b}} - \frac{\hbar\omega}{E}\mathbf{z} \right| - \log |\hat{\mathbf{b}} - \mathbf{z}| \right) \\ &\equiv -\frac{\Phi(\omega, \mathbf{z})}{\pi^2 |\mathbf{z}|^2 e^{i\lambda\phi_z}}, \end{aligned} \quad (2.14)$$

in which the function Φ turns out to be useful for the treatment of rescattering, too (Sec. II C). Furthermore, for relatively large angles [$|\boldsymbol{\theta}| \gg \theta_m \equiv \hbar/(Eb)$], Eq. (2.13) involves values of $\hbar\omega|\mathbf{z}|/E \lesssim \theta_m/|\boldsymbol{\theta}|$ which are uniformly small, and the expressions (2.14) can be replaced by their $\omega \rightarrow 0$ limits

$$\begin{aligned} h_s^{(\lambda)}(z) &= -\frac{\Phi_{\text{cl}}(z)}{\pi^2 |\mathbf{z}|^2 e^{i\lambda\phi_z}}, \\ \Phi_{\text{cl}}(z) &\equiv \lim_{\omega \rightarrow 0} \Phi = \hat{\mathbf{b}} \cdot \mathbf{z} + \log |\hat{\mathbf{b}} - \mathbf{z}|, \end{aligned} \quad (2.15)$$

which is the field occurring in the Regge amplitude (2.12); the modulating function Φ_{cl} appears also in the classical analysis of radiation [13].

The last aspect we have to take into account in order to determine the general $2 \rightarrow 3$ high-energy emission amplitude at lowest order is to consider the case of incoming particles with a generic direction of momenta. Since we always work in the c.m. frame, we parametrize $\vec{p}_1 = E(\boldsymbol{\Theta}_i, \sqrt{1 - \boldsymbol{\Theta}_i^2})$, where $\boldsymbol{\Theta}_i = |\boldsymbol{\Theta}_i|(\cos \phi_i, \sin \phi_i)$ is a 2D vector that describes both polar and azimuthal angles of the incoming particles. In Ref. [19], we proved the transformation formula for the generic helicity amplitude

$$\begin{aligned} \mathcal{M}^{(\lambda)}(\mathbf{b}, E, \boldsymbol{\theta}, \omega; \boldsymbol{\Theta}_i) &= e^{i\lambda(\phi_{\boldsymbol{\theta}} - \phi_{\boldsymbol{\theta} - \boldsymbol{\Theta}_i})} \mathcal{M}^{(\lambda)}(\mathbf{b}, E, \boldsymbol{\theta} - \boldsymbol{\Theta}_i, \omega; \mathbf{0}). \end{aligned} \quad (2.16)$$

By applying Eq. (2.16) to the matched amplitude (2.13), one immediately finds

$$\begin{aligned} \mathcal{M}_{\text{matched}}(\mathbf{b}, E, \boldsymbol{\theta}, \omega; \boldsymbol{\Theta}_i) &= \sqrt{\alpha_G} \frac{R}{2} e^{i\lambda\phi_{\boldsymbol{\theta}}} \\ &\quad \times \int d^2\mathbf{z} e^{i\mathbf{b}\omega\mathbf{z} \cdot (\boldsymbol{\theta} - \boldsymbol{\Theta}_i)} h_s^{(\lambda)}(\omega, \mathbf{z}), \end{aligned} \quad (2.17)$$

¹Notation: the 2D vectors $\mathbf{Q}, \mathbf{q}, \boldsymbol{\theta}, \mathbf{z}$, etc., are denoted with boldface characters; their complex representation, e.g., $z = z_1 + iz_2 = |z|e^{i\phi_z}$ is denoted with italic font. Note, however, that $b = |\mathbf{b}|$ is a real quantity.

and the whole Θ_i dependence amounts to a shift in the exponential factor.

C. Eikonal emission and rescattering

The physics of trans-Planckian scattering is captured, at leading level, by the resummation of eikonal diagrams, as illustrated in Sec. II A. In order to compute the associated graviton radiation, it is therefore mandatory to consider graviton emission from all ladder diagrams, as depicted in Fig. 3.

As we shew in Ref. [19], the crucial fact is that *all* internal lines insertions—for fast particles and exchanged particles alike—can be accounted for by calculating n diagrams for the eikonal contribution with n exchanged gravitons, where the *matched* amplitude (2.17) is inserted in turn in correspondence to the j th exchanged graviton (Fig. 3), adjusting for the local incidence angle $\Theta_i = \theta_{j-1}$.

The ladderlike structure of such an amplitude in momentum space is a convolution in the \mathbf{Q}_j -variables, with $\mathbf{Q}_1 + \dots + \mathbf{Q}_n = \mathbf{Q}$. Thus, in impact parameter space, the amplitude is obtained as a product of $j-1$ elastic amplitudes, the emission amplitude from the j th leg, and $n-j$ elastic amplitudes, the upper particle of which, by energy conservation, has reduced energy $E \rightarrow E - \hbar\omega$.

Let us express the elastic amplitude in terms of the dimensionless function $\Delta(\mathbf{b})$ such that

$$\begin{aligned} \mathcal{M}_{\text{el}}(\mathbf{b}, E) &= 2\delta(\mathbf{b}, s = 4EE') \\ &\equiv 2R \frac{E}{\hbar} \Delta(\mathbf{b}), \\ \Delta_0(\mathbf{b}) &= \log\left(\frac{L}{b}\right), \end{aligned} \quad (2.18)$$

so as to explicitly show the linear proportionality of the amplitude on the upper (jet 1) particle energy E (which varies after graviton emission). The energy E' of the lower particle (jet 2) stays unchanged, and its dependence has been absorbed in the constant $R = 4GE'$.

The n -rung amplitude for emission of a graviton with momentum q from the j th exchange of the ladder can then be expressed by the z -representation

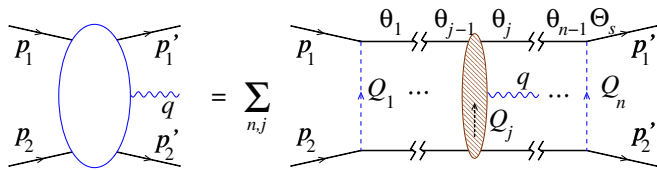


FIG. 3. Graviton emission from the eikonal ladder. The n -rung diagram with the emission from the j th exchange is denoted by $\mathcal{M}^{[n,j]}$ in the text.

$$\begin{aligned} &i\mathcal{M}_\lambda^{[n,j]}(\mathbf{b}, \omega, \boldsymbol{\theta}) \\ &= e^{i\lambda\phi_\theta} \sqrt{\alpha_G} \frac{R}{2} \frac{i^n}{n!} \int d^2z e^{i\mathbf{b}\omega\boldsymbol{\theta}\cdot\mathbf{z}} \\ &\times \left[\mathcal{M}_{\text{el}}\left(\mathbf{b} - \frac{\hbar\omega}{E} \mathbf{b}\mathbf{z}, E\right) \right]^{j-1} \\ &\times h_s^{(\lambda)}(\omega, z) [\mathcal{M}_{\text{el}}(\mathbf{b}, E - \hbar\omega)]^{n-j}. \end{aligned} \quad (2.19)$$

Note the effect of the incidence angle $\Theta_i = \theta_{j-1} = (\mathbf{Q}_1 + \dots + \mathbf{Q}_{j-1})/E$ in the exponent of Eq. (2.17) which, after Fourier transform, has shifted the impact parameters of the first elastic amplitudes by the amount $-\frac{\hbar\omega}{E} \mathbf{b}\mathbf{z}$. In addition, as already mentioned, the energy of the upper particle after the emission has the reduced value $E - \hbar\omega$, and this modifies the second argument of the elastic amplitudes after the emission.

Before summing all ladder diagrams, we take into account the rescattering of the emitted graviton with the external particles $p_j: j = 1, 2$. This interaction is proportional to $G(p_j + q)^2$ and is dominated by the exchange of gravitons between q and p_2 , since $(p_1 + q)^2 \sim \hbar\omega E |\boldsymbol{\theta} - \boldsymbol{\theta}_j|^2 \ll (p_2 + q)^2 \sim \hbar\omega E$ in the region of forward emission that we are considering. In practice, we add to the rightmost factor $[\mathcal{M}_{\text{el}}(\mathbf{b}, E - \hbar\omega)]^{n-j}$ in Eq. (2.19) [represented by the ladder of Fig. 4(a)] the contributions coming from rescattering diagrams where graviton exchanges between p_1 and p_2 are replaced by exchanges between q and p_2 in all possible ways [Figs. 4(b), 4(c), and 4(d)]. Since the ordering among eikonal exchanges and rescattering factors is irrelevant, the inclusion of such additional contributions amounts to the replacement ($N = n - j$)

$$\begin{aligned} [\mathcal{M}_{\text{el}}(\mathbf{b}, E - \hbar\omega)]^N &\rightarrow \sum_{r=0}^N \binom{N}{r} [\mathcal{M}_{\text{el}}(\mathbf{b}, E - \hbar\omega)]^{N-r} \\ &\times [\mathcal{M}_{\text{el}}(\mathbf{b} - \mathbf{x}, \hbar\omega)]^r \\ &= [\mathcal{M}_{\text{el}}(\mathbf{b}, E - \hbar\omega) + \mathcal{M}_{\text{el}}(\mathbf{b} - \mathbf{x}, \hbar\omega)]^N \\ &= \{2R[(E/\hbar - \omega)\Delta(\mathbf{b}) + \omega\Delta(\mathbf{b} - \mathbf{x})]\}^N, \end{aligned} \quad (2.20)$$

where we took into account that in diagrams with N exchanged gravitons there are $\binom{N}{r}$ distinct diagrams with r rescattering gravitons and that in each rescattering factor the energy of the upper particle (i.e., the emitted graviton) is $\hbar\omega$. Furthermore, we took into account that the transverse position of the emitted graviton with respect to the lower particle (i.e., p_2) is $\mathbf{b} - \mathbf{x}$, where $\mathbf{x} = \mathbf{b}\mathbf{z}$ is the variable conjugated to $\mathbf{q} = \omega\boldsymbol{\theta}$ [cf. Eq. (2.19)], hence to be interpreted as the transverse position of the emitted graviton with respect to p_1 .

Substituting the expression of Eq. (2.20) into Eq. (2.19), we can perform the sum over n and j of all diagrams with the aid of the formula

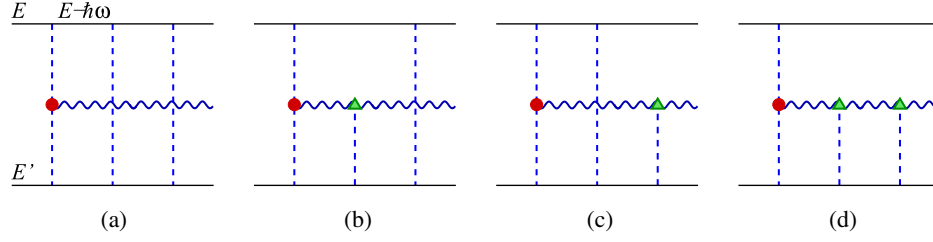


FIG. 4. Rescattering contributions (b,c,d) to eikonal graviton emission (a).

$$\sum_{n=1}^{\infty} \frac{1}{n!} \sum_{j=1}^n A^{j-1} B^{n-j} = \sum_{n=0}^{\infty} \frac{1}{n!} \frac{A^n - B^n}{A - B} = \frac{e^A - e^B}{A - B}. \quad (2.21)$$

It is also convenient to express the A and B quantities as the elastic amplitude (2.18) plus a quantum correction $\Phi_{A,B}$ as follows:

$$A \equiv i\mathcal{M}_{\text{el}}\left(\mathbf{b} - \frac{\hbar\omega}{E}\mathbf{x}, E\right) = 2i\alpha_G \left[\Delta(\mathbf{b}) + \frac{\hbar\omega}{E}\Phi_A(\mathbf{x}) \right]$$

$$B \equiv i[\mathcal{M}_{\text{el}}(\mathbf{b}, E - \hbar\omega) + \mathcal{M}_{\text{el}}(\mathbf{b} - \mathbf{x}, \hbar\omega)] \\ = 2i\alpha_G \left[\Delta(\mathbf{b}) + \frac{\hbar\omega}{E}\Phi_B(\mathbf{x}) \right]$$

$$\Phi_A(\mathbf{x}) \equiv \frac{E}{\hbar\omega} \left[\Delta\left(\mathbf{b} - \frac{\hbar\omega}{E}\mathbf{x}\right) - \Delta(\mathbf{b}) \right] \\ = -\Delta'(\mathbf{b}) \cdot \mathbf{x} + \mathcal{O}\left(\frac{\hbar\omega}{E}\right) \quad (2.22a)$$

$$\Phi_B(\mathbf{x}) \equiv \Delta(\mathbf{b} - \mathbf{x}) - \Delta(\mathbf{b}) = \Phi_A(\mathbf{x})|_{E \rightarrow \hbar\omega}. \quad (2.22b)$$

We note that the denominator in Eq. (2.21) is proportional to the Φ -function defined in Eq. (2.14),

$$A - B = 2i\alpha_G \frac{\hbar\omega}{E} [\Phi_A - \Phi_B] = 2i\omega R\Phi, \quad (2.23)$$

and is therefore intimately related to the soft field h_s .

From the technical point of view, such a relation provides the cancellation between h_s in Eq. (2.19) and the mentioned denominator $A - B$ of (2.21), to yield finally the one-graviton emission amplitude

$$i\mathcal{M}_\lambda(\mathbf{b}; \omega, \boldsymbol{\theta}) = e^{i\alpha_G 2\Delta(\mathbf{b})} \mathfrak{M}_\lambda(\mathbf{b}; \omega, \boldsymbol{\theta}) \\ \frac{\mathfrak{M}_\lambda(\mathbf{b}; \omega, \boldsymbol{\theta})}{e^{i\lambda\phi_\theta}} \equiv \sqrt{\alpha_G} \frac{R}{\pi} \int \frac{d^2z}{2\pi|z|^2} e^{i\lambda\phi_z} \\ \times e^{ib\omega\theta \cdot z} e^{2i\omega R\Phi_A} \frac{e^{-2i\omega R\Phi} - 1}{2i\omega R}, \quad (2.24)$$

which reduces to the classical expression (4.11) of Ref. [13] in the limit $\hbar\omega/E \rightarrow 0$, $\lambda = -2$ and $\Delta = \Delta_0$, since $\Phi \rightarrow \Phi_{\text{cl}}$ [cf. Eq. (2.15)] and $2R\Phi_A \rightarrow 2R\hat{\mathbf{b}} \cdot \mathbf{z} = -b\Theta_s \cdot \mathbf{z}$.

From the conceptual point of view, the identity (2.23) is surprising because it relates the exponents (which describe elastic plus rescattering exchanges) to the soft field $\sim \Phi$ (which describes graviton emission). The explanation lies in the derivation [19] of the soft-based representation (2.13) of which the form

$$\mathcal{M}_{\text{matched}} = \text{soft}|_E - \text{soft}|_{\hbar\omega} \simeq \text{Regge}|_E \quad (2.25)$$

has the alternative interpretations of external plus internal insertions in the soft-emission language and of elastic plus rescattering ones in the Regge language.

We shall base on that representation the generalized emission amplitude including subleading corrections, that will be investigated in Sec. III [Eqs. (3.26) and (3.29)].

D. Multigraviton emission and linear coherent state

In order to compute the multigraviton emission amplitude from eikonal ladder diagrams, let us start from the two-graviton emission process. We exploit again the \mathbf{b} -space factorization formula of Regge amplitudes. Referring to Fig. 5, if graviton 1 is emitted first from the j_1 th rung and then graviton 2 is emitted from the j_2 th rung ($j_1 < j_2$) of an n -rung ladder, the corresponding amplitude reads

$$i\mathcal{M}^{[n, (j_1 < j_2)]}(1, 2) = \frac{i^n}{2!n!} e^{i(\lambda_1\phi_{\theta_1} + \lambda_2\phi_{\theta_2})} \left(\sqrt{\alpha_G} \frac{R}{2} \right)^2 \\ \times \int d^2\mathbf{x}_1 d^2\mathbf{x}_2 e^{i(\omega_1\theta_1 \cdot \mathbf{x}_1 + \omega_2\theta_2 \cdot \mathbf{x}_2)} \\ \times A^{j_1-1} h_s(\mathbf{b}, \mathbf{x}_1, \omega_1) B^{j_2-j_1-1} \\ \times h_s(\mathbf{b}, \mathbf{x}_2, \omega_2) C^{n-j_2} \quad (2.26)$$

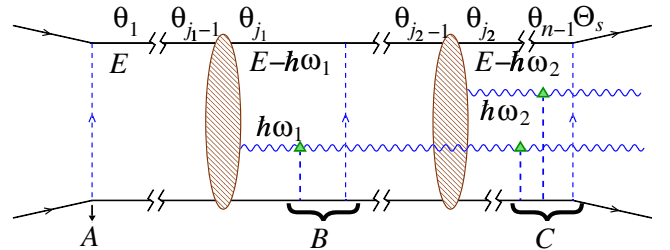


FIG. 5. Double-graviton emission from the eikonal ladder. A denotes eikonal exchanges before graviton emissions, B denotes eikonal exchanges and rescattering of graviton 1, and C includes also rescattering of graviton 2.

where, as before, the fields h_s describe real graviton production, while graviton exchanges and rescattering are encoded by the quantities

$$\begin{aligned} A &= i\mathcal{M}_{\text{el}}\left(\mathbf{b} - \frac{\hbar\omega_1\mathbf{x}_1 + \hbar\omega_2\mathbf{x}_2}{E}, E\right) \\ B &= i\mathcal{M}_{\text{el}}\left(\mathbf{b} - \frac{\hbar\omega_2}{E}\mathbf{x}_2, E - \hbar\omega_1\right) + i\mathcal{M}_{\text{el}}(\mathbf{b} - \mathbf{x}_1, \hbar\omega_1) \\ C &= i\mathcal{M}_{\text{el}}(\mathbf{b}, E - \hbar\omega_1 - \hbar\omega_2) + i\mathcal{M}_{\text{el}}(\mathbf{b} - \mathbf{x}_1, \hbar\omega_1) \\ &\quad + i\mathcal{M}_{\text{el}}(\mathbf{b} - \mathbf{x}_2, \hbar\omega_2). \end{aligned} \quad (2.27)$$

The quantity A denotes the eikonal exchanges before any graviton emission and is given by the elastic amplitude \mathcal{M}_{el} with a shift in its first argument due to the effect of the incidence angles $\Theta_{j_1-1}, \Theta_{j_2-1}$ of both gravitons, an effect that propagates backward in the ladder, as explained in the previous section.

The quantity B describes the interactions occurring in the middle of the ladder, i.e., after the emission of graviton 1 and before that of graviton 2. It consists in the sum of two terms: the first one describes the eikonal exchanges between p_1 and p_2 and includes both the effect of the incidence angle Θ_{j_2-1} (shift in the first argument) and also the reduced gravitational coupling $E \rightarrow E - \hbar\omega_1$ in the upper vertices due to energy conservation. The second term describes the rescattering of graviton 1 with p_2 .

Finally, the first of the three terms building C represents the eikonal exchanges between p_1 and p_2 with reduced coupling $E \rightarrow E - \hbar(\omega_1 + \omega_2)$ in the upper vertices, while the other two terms take into account rescattering corrections of both gravitons.

The sum over all such ladder diagrams amounts to

$$\begin{aligned} \mathfrak{S}(1, 2) &\equiv \sum_{n=2}^{\infty} \frac{1}{n!} \sum_{j_1=1}^{n-1} \sum_{j_2=j_1+1}^n A^{j_1-1} B^{j_2-j_1-1} C^{n-j_2} \\ &= \frac{e^A}{(A-B)(A-C)} + \frac{e^B}{(B-A)(B-C)} \\ &\quad + \frac{e^C}{(C-A)(C-B)}. \end{aligned} \quad (2.28)$$

By swapping the graviton indices $1 \leftrightarrow 2$, one immediately obtains the symmetric contribution with graviton 2 emitted “before” graviton 1.

Now, the sum of these two contributions does not factorize exactly in two independent factors. It would if $A - B = [B - C]_{1 \leftrightarrow 2}$, but this is not the case. However, $A - B = [B - C]_{1 \leftrightarrow 2} + \mathcal{O}(A\hbar^2\omega_i^2/E^2)$; therefore, factorization can be recovered by neglecting contributions of relative order $\mathcal{O}(\hbar^2\omega_i^2/E^2)$. In fact, thanks to Eqs. (2.22), we have

$$\begin{aligned} A &= 2i\alpha_G\Delta\left(\mathbf{b} - \frac{\hbar\omega_1\mathbf{x}_1 + \hbar\omega_2\mathbf{x}_2}{E}\right) \\ &= 2i\alpha_G\left[\Delta(\mathbf{b}) - \Delta'(\mathbf{b}) \cdot \frac{\hbar\omega_1\mathbf{x}_1 + \hbar\omega_2\mathbf{x}_2}{E} + \mathcal{O}\left(\frac{\hbar^2\omega_i^2}{E^2}\right)\right] \\ &= 2i\{\alpha_G\Delta(\mathbf{b}) + \omega_1 R\Phi_A(\mathbf{x}_1) + \omega_2 R\Phi_A(\mathbf{x}_2) + \mathcal{O}(G\hbar^2\omega_i^2)\} \\ B &= 2i\alpha_G\left[\left(1 - \frac{\hbar\omega_1\mathbf{x}_1}{E}\right)\Delta\left(\mathbf{b} - \frac{\hbar\omega_2\mathbf{x}_2}{E}\right) + \frac{\hbar\omega_1\mathbf{x}_1}{E}\Delta(\mathbf{b} - \mathbf{x}_1)\right] \\ &= 2i\{\alpha_G\Delta(\mathbf{b}) + \omega_2 R\Phi_A(\mathbf{x}_2) + \omega_1 R\Phi_B(\mathbf{x}_1) + \mathcal{O}(G\hbar^2\omega_i^2)\} \\ C &= i2\alpha_G\left[\left(1 - \frac{\hbar\omega_1\mathbf{x}_1}{E} - \frac{\hbar\omega_2\mathbf{x}_2}{E}\right)\Delta(\mathbf{b}) + \frac{\hbar\omega_1\mathbf{x}_1}{E}\Delta(\mathbf{b} - \mathbf{x}_1) \right. \\ &\quad \left. + \frac{\hbar\omega_1\mathbf{x}_2}{E}\Delta(\mathbf{b} - \mathbf{x}_2)\right] \\ &= 2i\{\alpha_G\Delta(\mathbf{b}) + \omega_1 R\Phi_B(\mathbf{x}_1) + \omega_2 R\Phi_B(\mathbf{x}_2)\}. \end{aligned} \quad (2.29)$$

By noting that the elastic amplitude $e^{2i\alpha_G\Delta(\mathbf{b})}$ is a common factor in all exponentials, we can approximate the infinite sum (2.28) in the form

$$\mathfrak{S}(1, 2) \simeq e^{2i\alpha_G\Delta}\left[\frac{e^{\varphi_{A1}+\varphi_{A2}}}{\varphi_1(\varphi_1+\varphi_2)} - \frac{e^{\varphi_{B1}+\varphi_{A2}}}{\varphi_1\varphi_2} + \frac{e^{\varphi_{B1}+\varphi_{B2}}}{(\varphi_1+\varphi_2)\varphi_2}\right], \quad (2.30)$$

where we used the shortcuts $\varphi_{A1} \equiv 2i\omega_1 R\Phi_A(\mathbf{x}_1)$ and analogous ones.

At this point, it is straightforward to check that

$$\mathfrak{S}(1, 2) + \mathfrak{S}(2, 1) \simeq e^{2i\alpha_G\Delta} \frac{e^{\varphi_{A1}}(e^{-\varphi_1} - 1)}{\varphi_1} \frac{e^{\varphi_{A2}}(e^{-\varphi_2} - 1)}{\varphi_2} \quad (2.31)$$

and to obtain the two-graviton emission amplitude in the factorized form,

$$\begin{aligned} &i\mathcal{M}_{\lambda_1\lambda_2}(\mathbf{b}; \omega_1, \boldsymbol{\theta}_1; \omega_2, \boldsymbol{\theta}_2) \\ &\simeq e^{i\alpha_G 2\Delta(\mathbf{b})} \mathfrak{M}_{\lambda_1}(\mathbf{b}; \omega_1, \boldsymbol{\theta}_1) \mathfrak{M}_{\lambda_2}(\mathbf{b}; \omega_2, \boldsymbol{\theta}_2), \end{aligned} \quad (2.32)$$

in terms of the one-graviton amplitude and of the elastic S -matrix. It is clear from Eqs. (2.29) that such an approximate relation neglects terms of relative order $\mathcal{O}(\hbar^2\omega^2/E^2) = \mathcal{O}(\omega R/\alpha_G)^2$, which are negligible in the regime we are considering and are subleading not only with respect to terms $\sim\alpha_G$ [like the eikonal phase $\delta(\mathbf{b})$] but also with respect to the terms $\sim\omega R$.

We expect an analogous factorization formula to hold for the generic N -graviton emission amplitude off eikonal ladders (we explicitly checked the three-graviton case), in the form

$$i\mathcal{M}(\mathbf{b}; q_1, \dots, q_N) \simeq e^{i\alpha_G 2\Delta(b)} \prod_{r=1}^N \mathfrak{M}_{\lambda_r}(\mathbf{b}; \omega_r, \boldsymbol{\theta}_r). \quad (2.33)$$

Such an independent emission pattern corresponds to the final state

$$|\text{gravitons; out}\rangle = \sqrt{P_0} \exp \left\{ \int \frac{d^3 q}{\hbar^3 \sqrt{2\omega}} 2i \sum_{\lambda} \mathfrak{M}_{\lambda}(\mathbf{b}, \vec{q}) a_{\lambda}^{\dagger}(\vec{q}) \right\} |0\rangle \quad (2.34)$$

in the Fock space of gravitons, with $P_0 = 1$, and creation ($a_{\lambda}^{\dagger}(\vec{q})$) and destruction [$a_{\lambda}(\vec{q})$] operators of definite helicity λ are normalized to a wave number δ -function commutator [$a_{\lambda}(\vec{q}), a_{\lambda'}^{\dagger}(\vec{q}')$] = $\hbar^3 \delta^3(\vec{q} - \vec{q}') \delta_{\lambda\lambda'}$. However, this state takes into account only real emission. Virtual corrections can then be incorporated by exponentiating both creation and destruction operators in a (unitary) coherent-state operator acting on the graviton vacuum $|0\rangle$ (the initial state of gravitons). We thus obtain the full S -matrix

$$\hat{S} = e^{2i\delta} \exp \left\{ \int \frac{d^3 q}{\hbar^3 \sqrt{2\omega}} 2i \left[\sum_{\lambda} \mathfrak{M}_{\lambda}(\mathbf{b}, \vec{q}) a_{\lambda}^{\dagger}(\vec{q}) + \text{H.c.} \right] \right\} \quad (2.35)$$

that is unitary, because of the anti-Hermitian exponent, when $b > b_c$.

By normal ordering Eq. (2.35) when acting on the initial state $|0\rangle$, we find that the final state of the graviton is still given by Eq. (2.34), but with P_0 given by

$$P_0 = \exp \left\{ -2 \int \frac{d^3 q}{\hbar^3 \omega} \sum_{\lambda} |\mathfrak{M}_{\lambda}(\mathbf{b}, \vec{q})|^2 \right\}, \quad (2.36)$$

which is just the no-emission probability, coming from the a, a^{\dagger} commutators.

Due to the factorized structure of Eq. (2.34), it is straightforward to derive the inclusive distributions of gravitons and even their generating functional

$$\mathcal{G}[z_{\lambda}(\vec{q})] = \exp \left\{ 2 \int_{\Delta\omega} \frac{d^3 q}{\hbar^3 \omega} \sum_{\lambda} |\mathfrak{M}_{\lambda}^{(\lambda)}(\vec{q})|^2 [z_{\lambda}(\vec{q}) - 1] \right\}. \quad (2.37)$$

In particular, the polarized energy emission distribution in the solid angle Ω and its multiplicity density are given by

$$\begin{aligned} \frac{dE_{\lambda}^{\text{GW}}}{d\omega d\Omega} &= \hbar\omega \frac{d\mathcal{N}_{\lambda}}{d\omega d\Omega} = 2\omega^2 \hbar |\mathfrak{M}_{\lambda}(\mathbf{b}, \vec{q})|^2, \\ \frac{d\mathcal{N}}{d\omega} &= p(\omega) = \frac{1}{\hbar\omega} \frac{dE^{\text{GW}}}{d\omega}. \end{aligned} \quad (2.38)$$

Both quantities will be discussed in the next section.

E. Large ωR emission amplitude

In this section, we analyze the graviton emission amplitude (2.24) and its spectrum (2.38) generated by a small-angle ($\Theta_s \ll 1$) scattering in the frequency region $\omega \gtrsim R^{-1}$ and in the classical limit $\hbar\omega \ll E$.

We recall that the frequency spectrum integrated in the solid angle was already studied in Ref. [19] for large impact parameters $b \gg R$, i.e., for small deflection angles $\Theta_s \ll 1$, both with and without rescattering corrections. We briefly report the main results:

- (i) For $\omega R \lesssim \Theta_s$, the spectrum is flat and agrees with the zero-frequency limit (ZFL).
- (ii) For $\Theta_s \lesssim \omega R \lesssim 1$, the spectrum shows a slow (logarithmic) decrease with frequency. The behavior in these two regions is rather insensitive to the inclusion of rescattering and can be summarized by

$$\begin{aligned} \frac{dE^{\text{GW}}}{d\omega} &\simeq G_s \Theta_E^2 \left[\frac{2}{\pi} \log \min \left(\frac{1}{\Theta_s}, \frac{1}{\omega R} \right) + \text{const} \right] \\ &(\omega R \lesssim 1). \end{aligned} \quad (2.39)$$

- (iii) For $\omega R \gtrsim 1$, the amplitude (2.24) is dominated by small- z values, and the z -integration can be safely extended to arbitrary large values without introducing spurious effects. The frequency distribution of radiated energy can then be well approximated by computing the square modulus of the amplitude (2.24) by means of the Parseval identity, yielding

$$\begin{aligned} \frac{dE^{\text{GW}}}{d\omega} &= 2G_s \frac{\Theta_E^2}{\pi^2} \int \frac{d^2 z}{|z|^4} \left(\frac{\sin \omega R \Phi(z)}{\omega R} \right)^2 \\ &(\omega R \gtrsim 1), \end{aligned} \quad (2.40)$$

the asymptotic behavior of which provides a spectrum decreasing like $1/\omega$; more precisely,

$$\frac{dE^{\text{GW}}}{d\omega} \simeq G_s \Theta_E^2 \frac{1}{\pi \omega R} \quad (\omega R \gg 1). \quad (2.41)$$

In this region, the inclusion of rescattering has the effect of lowering the spectrum by about 20%. In any case, the total radiated-energy fraction up to the kinematical bound $\omega_M = E/\hbar$ becomes

$$\frac{E^{\text{GW}}}{\sqrt{s}} = \frac{\Theta_E^2}{2\pi} \log \alpha_G \quad (2.42)$$

and may exceed unity, thus signalling the need for energy-conservation corrections at sizeable angles (cf. Sec. IV).

In Fig. 6, we show the energy spectrum (divided by $G_s \Theta_E^2$) for various values of Θ_s . It is apparent that, for $\omega R \gg 1$, its shape is almost independent of Θ_s . As we will show in

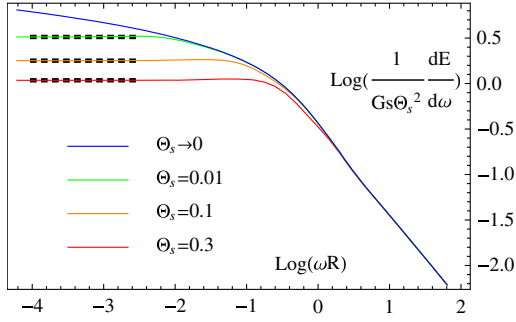


FIG. 6. Frequency spectrum of gravitational radiation for various values of Θ_s . For each $\Theta_s > 0$, the ZFL value $\frac{2}{\pi} \log(1.65/\Theta_s)$ is obtained (dashed lines).

Sec. III, there will be qualitative differences when approaching the strong-coupling region $\Theta_s \sim 1$ where subleading contributions become important.

On the contrary, the angular distribution of graviton radiation studied in Ref. [19] did not take into account rescattering contributions. The latter are actually irrelevant for $\omega R \ll 1$ but change drastically the angular pattern for $\omega R \gg 1$. In fact, the graviton exchanges between the outgoing graviton q and p_2 (see Fig. 4) have the main effect of deflecting the direction of q , just like the eikonal exchanges between p_1 and p_2 are responsible for the deflection of p_1 (and p_2). It turns out that the graviton radiation is collimated around the direction Θ_s of the outgoing particle(s).

Quantitatively, the resummed emission amplitude (2.24) in the classical limit $\hbar\omega \ll E$ and, say, for helicity $\lambda = -2$ reads

$$\begin{aligned} \mathfrak{M}_{\text{cl}}(\mathbf{b}, \boldsymbol{\theta}) &= \sqrt{\alpha_G} \frac{R}{\pi} e^{-2i\phi_\theta} \\ &\times \int \frac{d^2z}{2\pi z^{*2}} \frac{e^{i\omega b z \cdot (\boldsymbol{\theta} - \boldsymbol{\Theta}_s)}}{2i\omega R} (e^{-2i\omega R \Phi_{\text{cl}}(z)} - 1), \end{aligned} \quad (2.43)$$

where $\boldsymbol{\Theta}_s$ is the fast-particle scattering angle and Φ_{cl} was defined in Eq. (2.15). We are interested in evaluating such an amplitude at large ωR . Since in the second exponential the function

$$\Phi_{\text{cl}}(z) \equiv \hat{\mathbf{b}} \cdot \mathbf{z} + \log|\hat{\mathbf{b}} - \mathbf{z}| = \frac{1}{2}(z_2^2 - z_1^2) + \mathcal{O}(|z|^3) \quad (2.44)$$

vanishes (quadratically) at the origin, we expect that for $\omega R \gg 1$ the dominant contributions to the amplitude come from the small- z integration region. By substituting the second-order expansion (2.44) into Eq. (2.43) and by rescaling the integration variable $\sqrt{\omega R} z \equiv Z \equiv x + iy$, we obtain

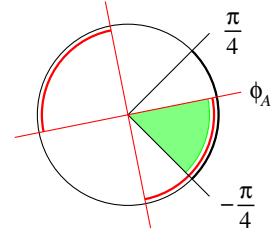


FIG. 7. The end points in the integral (2.47) correspond to the angular interval $[\phi_1, \phi_2]$ (green region), the latter being determined by the intersection of the $[-\pi/4, \pi/4]$ interval (black sector) with the region where $\sin(2(\phi_A - \phi))$ is positive (red sectors).

$$\frac{2\pi\omega\mathfrak{M}}{\sqrt{\alpha_G} e^{-2i\phi_\theta}} \equiv I(\mathbf{A}) = \int \frac{d^2Z}{2\pi Z^{*2}} e^{i2\mathbf{A} \cdot \mathbf{Z}} [e^{i(x^2 - y^2)} - 1] \frac{1}{i}, \quad (2.45)$$

which is a function of the two-dimensional variable,

$$\begin{aligned} \mathbf{A} &\equiv |\mathbf{A}|(\cos \phi_A, \sin \phi_A) \equiv \sqrt{\omega R} \frac{\boldsymbol{\theta} - \boldsymbol{\Theta}_s}{|\boldsymbol{\Theta}_s|}, \\ \mathbf{A} &\equiv |\mathbf{A}| e^{i\phi_A} \in \mathbb{C}. \end{aligned} \quad (2.46)$$

Were it not for the factor Z^{*2} in the denominator, the rhs of Eq. (2.45) would have the structure of a Gaussian integral in two dimensions. It is possible, however, to provide a simple one-dimensional integral representation for the function $I(\mathbf{A})$ in Eq. (2.45) (see Appendix B),

$$I(\mathbf{A}) = -\frac{\mathbf{A}}{2\mathbf{A}^*} \int_{\zeta_1}^{\zeta_2} \frac{d\zeta}{\zeta^2} e^{-\frac{1}{2}\mathbf{A}^* \zeta^2 (\zeta^2 + 1)}, \quad (2.47)$$

where the complex-integration end points $\zeta_l \equiv e^{i2\phi_l} : l = 1, 2$ are determined by the azimuth ϕ_A , i.e., the azimuth of $\boldsymbol{\theta}$ with respect to $\boldsymbol{\Theta}_s$, according to Fig. 7. The function $I(\mathbf{A})$ satisfies some symmetry properties, and in particular, it vanishes for $\phi = -\pi/4 + n\pi : n \in \mathbb{Z}$. This relation follows from the fact that, for $\phi_A = (n - \frac{1}{4})\pi : n \in \mathbb{Z}$, the integration limits in Eq. (2.47) coincide and thus the integral vanishes.

The intensity of the radiation on the tangent space of angular directions centered at $\boldsymbol{\theta} = \boldsymbol{\Theta}_s$ and parametrized by \mathbf{A} is shown in Fig. 13(a). The main part of the radiation in the forward hemisphere is concentrated around $|\mathbf{A}| \lesssim 1$, which means $|\boldsymbol{\theta} - \boldsymbol{\Theta}_s| \lesssim |\boldsymbol{\Theta}_s|/\sqrt{\omega R}$, and is more and more collimated around the direction $\boldsymbol{\Theta}_s$ of the outgoing particle 1 for larger and larger ωR . This feature is a direct consequence of rescattering processes, through which the emitted gravitons feel the gravitational attraction of particle 2 and are therefore deflected, on average, in the same way as particle 1.

At given values of helicity and frequency, we observe a peculiar interference pattern, with a vanishing amplitude at $\phi_A = \pm\pi/4 + n\pi$ for helicity ± 2 . Such interference fringes

are washed out when integrating the intensity over some frequency range and summing over helicities. On the whole, the radiation intensity is distributed almost isotropically around Θ_s , with an azimuthal periodicity (in ϕ_A) resembling a quadrupolar shape.

This angular distribution differs from our prediction in Ref. [19], where we neglected rescattering and found graviton radiation distributed in the scattering plane with angles ranging from zero (incoming particle 1) to Θ_s (outgoing particle 1). By comparison, rescattering produces the above dependence on $\theta - \Theta_s$, by associating in a clearer way jet 1 to the outgoing particle 1.

Graviton radiation associated to large-angle ($|\Theta_s| \sim 1$) scattering will be analyzed in Sec. IV and compared to the previous one.

III. RADIATION MODEL WITH ACV RESUMMATION

In this section, we extend the treatment of graviton radiation to scattering processes characterized by large deflection angles $\Theta_s = \mathcal{O}(1)$ or, equivalently, to impact parameters $b \sim R$ of the order of the gravitational radius, where the gravitational interaction becomes strong and a collapse is expected to occur, at least at the classical level. This requires going beyond the leading eikonal approximation reviewed in Sec. II and to take into account the nonlinear interactions which dominate at high energy. Such corrections to the eikonal approximation have been identified [7,8] and studied in detail for elastic scattering [9,30–32]. Their treatment is based on an effective action model that we are going to summarize in Sec. III A and to apply to graviton radiation in the rest of the section.

A. Reduced-action model

The model consists in a shock-wave solution of the effective field theory proposed by ACV [8] in the regime $R \gg l_s$ of trans-Planckian scattering on the basis of Lipatov's action [29]. The effective metric fields of that solution have basically longitudinal (h_{++}, h_{--}) and transverse ($h_{ij}; i, j = 1, 2$) components of the form

$$\begin{aligned} h_{--} &= 2\pi R a(\mathbf{x}) \delta(x^-), \\ h_{++} &= 2\pi R \bar{a}(\mathbf{x}) \delta(x^+), \\ h &= \text{Tr}(h_{ij}) = \nabla^2 \phi(\mathbf{x}) \frac{1}{2} \Theta(x^+ x^-), \end{aligned} \quad (3.1)$$

where we note wave fronts of Aichelburg-Sexl type [33] with profile functions a and \bar{a} and an effective transverse field with support in $x^+ x^- > 0$.

A simplified formulation of the solution (3.1) was obtained in Ref. [9] by an azimuthal averaging procedure which relates it to a one-dimensional model in a transverse radial space with the axisymmetric action

$$\begin{aligned} \mathcal{A} &= 2\pi^2 G s \int dr^2 \left[\bar{s}a + s\bar{a} - 2\rho\dot{a} - \frac{2}{(2\pi R)^2} (1 - \dot{\rho})^2 \right] \\ &\left(\cdot \equiv \frac{d}{dr^2} \right) \end{aligned} \quad (3.2)$$

in which r^2 plays the role of time parameter. Here, $\phi(r^2)$ is replaced by the auxiliary field $\rho(r^2)$ —a sort of renormalized squared distance—defined by

$$\begin{aligned} \rho &\equiv r^2 [1 - (2\pi R)^2 \dot{\phi}], \\ h &\equiv \nabla^2 \phi = 4 \frac{d}{dr^2} (r^2 \dot{\phi}) \\ &= \frac{1}{(\pi R)^2} (1 - \dot{\rho}), \end{aligned} \quad (3.3)$$

which incorporates the basic ϕ , a , \bar{a} interaction, with effective coupling R^2 . Furthermore, the axisymmetric sources $s(r^2) = \delta(r^2)/\pi$ and $\bar{s}(r^2) = \delta(r^2 - b^2)/\pi$ describe (approximately) the energetic incident particles, and $\phi(r^2)$ is taken to be real valued—as for the transverse-traceless (TT) polarization only—thus neglecting the infrared singular one in the frequency range $\omega \sim 1/R$ we are interested in.

The equations of motion of (3.2) for the profile functions admit two constants of motion, yielding the relations

$$\dot{a} = -\frac{1}{2\pi\rho}, \quad \dot{\bar{a}} = -\frac{1}{2\pi\rho} \Theta(r^2 - b^2), \quad (3.4)$$

while that for the field ρ yields

$$\begin{aligned} \dot{\rho} &= 2(\pi R)^2 \dot{a} \dot{\bar{a}} = \frac{R^2}{2\rho^2} \Theta(r^2 - b^2), \\ \dot{\rho}^2 + \frac{R^2}{\rho} &= 1 \quad (r > b). \end{aligned} \quad (3.5)$$

The latter describe the r^2 -motion of $\rho(r^2)$ in a Coulomb field, which is repulsive for $\rho > 0$, and acts for $r^2 > b^2$ only, so that b^2 actually cuts off that repulsion in the short-distance region.

The interesting solutions of (3.4) and (3.5) are those which are ultraviolet safe—for which the effective field theory makes sense—and are restricted by the regularity condition $\rho(0) = 0$ which avoids a possible $r^2 = 0$ singularity of the ϕ -field.

External ($r > b$) and internal ($0 < r < b$) regular solutions are easily written down for this solvable model,

$$\begin{aligned} \rho &= \begin{cases} R^2 \cosh^2 \chi(r^2) & (r^2 \geq b^2) \\ \rho(b^2) + \dot{\rho}(b^2)(r^2 - b^2) & (0 \leq r^2 \leq b^2) \end{cases} \\ r^2 &= b^2 + R^2(\chi + \sinh \chi \cosh \chi - \chi_b - \sinh \chi_b \cosh \chi_b) \\ &(\chi_b \equiv \chi(b^2)) \end{aligned} \quad (3.6)$$

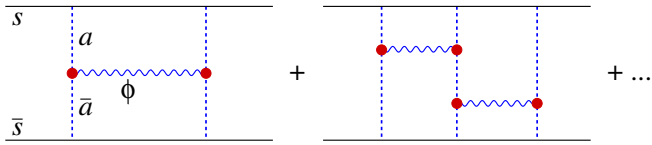


FIG. 8. The H diagram (left) and the first multi-H diagram (right) starting the series of subleading contributions to the eikonal.

and are matched at $r^2 = b^2$ by the condition ($t_b \equiv \tanh \chi_b$)

$$\begin{aligned} \rho(b^2) &= R^2 \cosh^2 \chi_b = b^2 \dot{\rho}(b^2) = b^2 t_b, \\ \frac{R^2}{b^2} &= t_b (1 - t_b^2). \end{aligned} \quad (3.7)$$

The criticality equation (3.7) is cubic in the t_b parameter and determines the branches of possible solutions with $\rho(0) = 0$. For $b^2 > b_c^2 \equiv (3\sqrt{3}/2)R^2$, there are two real-valued, non-negative solutions, and the ‘‘perturbative’’ one with $t_b \rightarrow 1$ for $b \gg b_c$ is to be taken. By replacing such a solution in the action (3.2), we get the nonperturbative on-shell expression

$$\begin{aligned} 2\delta(b, s) \equiv \mathcal{A} &= \alpha_G \int_0^{L^2} \frac{dr^2}{R^2}, \\ &\times \left[\frac{R^2}{\rho} \Theta(r^2 - b^2) - (1 - \dot{\rho})^2 \right] \\ &= \alpha_G \left[2\chi_L - 2\chi_b + 1 - \frac{1}{t_b} \right] \quad (b > b_c), \end{aligned} \quad (3.8)$$

where L is an IR cutoff needed to regularize the Coulomb singularity. The phase shift (3.8) shows the large- b behavior

$$\delta(b, s) \simeq \alpha_G \left(\log \frac{L}{b} + \frac{R^2}{4b^2} + \dots \right), \quad (3.9)$$

which, however, is only qualitatively correct for the subleading term of which the full expression is actually [7]

$$\Re \delta_H = \delta(b, s) - \alpha_G \log \frac{L}{b} = \alpha_G \frac{R^2}{2b^2}. \quad (3.10)$$

The difference is due to the various approximations being made (one polarization and azimuthal averaging).

Despite such approximations, the importance of the nonperturbative expressions (3.6) and (3.8) for solutions and action is to provide a resummation of all subleading contributions $\sim (R^2/b^2)^n$ to the eikonal of multi-H type (Fig. 8) and to exhibit its singularity structure in the classical collapse regime, on the basis of the criticality equation (3.7).

In fact, for $b < b_c$, we find that no real-valued solutions exist and t_b acquires an imaginary part. The solution with negative $\Im t_b$ has $\Im \mathcal{A} > 0$, is stable, and is close to the

perturbative solution at large distances. The corresponding action is found to yield a suppression of the elastic channel of the type

$$|S_{\text{el}}(b, s)|^2 \simeq \exp \left\{ -\frac{4\sqrt{2}}{3} \alpha_G \left(1 - \frac{b^2}{b_c^2} \right)^{3/2} \right\}, \quad (3.11)$$

which can be related to a tunnel effect [30,31] through the repulsive Coulomb-potential barrier which is classically forbidden.

Actually, the action shows a branch-point singularity at $b = b_c$ of index 3/2 with the expansion

$$\begin{aligned} \mathcal{A} - \mathcal{A}_c &= \alpha_G \left[\sqrt{3} \left(1 - \frac{b^2}{b_c^2} \right) \pm i \frac{2\sqrt{2}}{3} \left(1 - \frac{b^2}{b_c^2} \right)^{3/2} + \dots \right], \\ t_b &= \frac{1}{\sqrt{3}} \mp i \frac{\sqrt{2}}{3} \sqrt{1 - \frac{b^2}{b_c^2}} + \dots, \end{aligned} \quad (3.12)$$

which is thus responsible for the suppression (3.11) just mentioned. The presence of the index 3/2 seems a robust feature of this kind of model because the expansion of the action in t_b starts at order $(t_b - 1/\sqrt{3})^2$, due to the action stationarity, thus avoiding a square-root behavior.

The result so obtained is puzzling, however, because it may lead to unitarity loss [31,32], unless some additional state, or radiation enhancement, is found in the $b \leq b_c$ region. In fact, it represents a basic motivation of the present paper and of the following treatment of the radiation associated to the ACV resummation.

B. Single-graviton emission by H-diagram exchange

Here, we want to argue that the graviton radiation associated to the H-diagram eikonal exchange is well described by a generalization of the soft-based representation in Eq. (2.13). To this purpose, we shall use the dispersive method of Ref. [7], which consists in relating both (a) exchange and (b) emission to the multi-Regge amplitudes [15,29] pictured in the overlap functions of Fig. 9.

For the H diagram [Fig. 9(a)], the CCV helicity amplitude [15] for emitting a graviton of momentum $q' = q_2 - q_1$

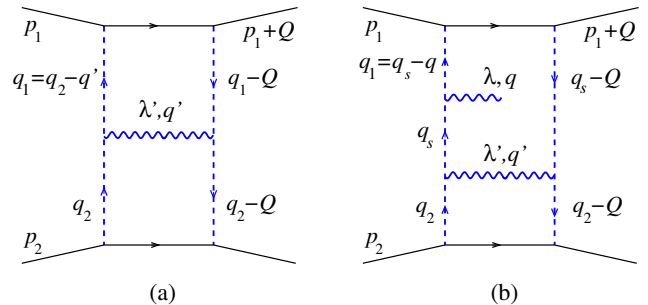


FIG. 9. (a) H diagram kinematics and (b) Graviton emission from the H diagram.

and helicity λ' , in the center-of-mass frame with incident momentum along the \hat{z} axis, is given by [cf. Eq. (2.11)]

$$M_{\text{Regge}}(\mathbf{q}', E, \omega, \mathbf{q}_2) = \frac{\kappa^2 s^2 J_L^{\mu\nu} \epsilon_{\mu\nu}^{(\lambda')}}{(\mathbf{q} - \mathbf{q}_2)^2 q_2^2} = \frac{\kappa^3 s^2}{q'^2} F^{(\lambda')}(\mathbf{q}_2, \mathbf{q}_2 - \mathbf{q}') \\ F^{(\lambda)}(\mathbf{q}_2, \mathbf{q}_1) \equiv 1 - e^{i\lambda(\phi_{\mathbf{q}_2} - \phi_{\mathbf{q}_1})}. \quad (3.13)$$

Correspondingly, the overlap function [Fig. 9(a)], at generally nonvanishing momentum transfer \mathbf{Q} and for the incidence direction along the \hat{z} axis in the center-of-mass frame, is proportional to the Lipatov graviton kernel [29]

$$K(\mathbf{q}_2, \mathbf{q}_1; \mathbf{Q}) \equiv \sum_{\lambda'} J_L^{\mu\nu}(\mathbf{q}_1, \mathbf{q}_2) \epsilon_{\mu\nu}^{(\lambda')}(\mathbf{q}') J_L^{\mu'\nu'}(\mathbf{q}_1', \mathbf{q}_2') \epsilon_{\mu'\nu'}^{(\lambda')*}(\mathbf{q}'), \quad (3.14)$$

where J_L is the Lipatov current [29] and $\mathbf{q}'_i \equiv \mathbf{q}_i - \mathbf{Q}$; $i = 1, 2$. In two transverse dimensions, where the \mathbf{q}_i 's are all coplanar, the explicit result is

$$K(\mathbf{q}_2, \mathbf{q}_1; \mathbf{Q}) = \frac{4q_1^2 q_2^2 q_1'^2 q_2'^2}{[(\mathbf{q}_1 - \mathbf{q}_2)^2]^2} \\ \times 2 \sin \phi_{12} \sin \phi_{1'2'} \cos(\phi_{12} - \phi_{1'2'}) \quad (3.15)$$

and checks with Ref. [29].

The result (3.15) is valid for on-shell intermediate particles and provides directly, by integration over \mathbf{q}_i and the Fourier transform in \mathbf{Q} to \mathbf{b} -space, the imaginary part of the H-diagram amplitude, or [9]

$$\Im \delta_H(b, s) \equiv Y G s R^2 \int d^2 \mathbf{q}' |\tilde{h}(\mathbf{b}, \mathbf{q}')|^2, \quad (3.16)$$

where

$$\tilde{h}(\mathbf{b}, \mathbf{q}) = 2 \int \frac{d^2 \mathbf{q}_2}{(2\pi)^2} \frac{e^{i\mathbf{b}\cdot\mathbf{q}_2}}{|\mathbf{q}|^2} [1 - e^{2i(\phi_{\mathbf{q}_2} - \phi_{\mathbf{q}_2'})}], \quad (3.17)$$

is the h -field in \mathbf{q} -space at $\lambda' = -2$ [15,19].² The quantity (3.17) has a logarithmic divergence, because of the known residual infrared singularity $\sim 1/|\mathbf{q}|^2$ of the integrand in (3.16), due to the longitudinal-transverse (LT) polarization. Such a divergence is expected and is compensated in observables by real emission in the usual way, so as to lead to finite, but resolution-dependent, results.

On the other hand, we are looking for $\Re \delta_2$, the H-diagram contribution to the two-loop eikonal, which is supposed to be IR safe, because a \mathbf{b} -dependent IR divergence would be observable and inconsistent with the

²The quantities $h = \text{Tr}(h_{ij}) \rightsquigarrow h_{zz^*}$ and $h_s \rightsquigarrow h_{zz}$, $h_{z^*z^*}$ are related to different components of the metric fields $h_{\mu\nu} \equiv g_{\mu\nu} - \eta_{\mu\nu}$ in the shock-wave solution (3.1). For a more precise identification, see Ref. [19].

Block-Nordsieck factorization theorem. In Ref. [7], it was shown that fixed-order dispersion relations plus S -matrix exponentiation lead indeed to the finite result

$$\Re \delta_2(b, s) = \frac{\pi}{2Y} \Im \delta_H(b, s) \Big|_{\text{Reg}} \\ = \frac{\pi}{2} G s R^2 \int d^2 \mathbf{q}' |\tilde{h}(\mathbf{b}, \mathbf{q}')|_{\text{Reg}}^2 \stackrel{b \gg R}{\approx} \alpha_G \frac{R^2}{2b^2} \\ = \frac{2G^3 s^2}{b^2}. \quad (3.18)$$

Here, the regularization subtraction is due to the second-order contributions of δ_0 and δ_1 to the S -matrix exponential.

Our present purpose is actually to compute the graviton radiation associated to the H diagram, in which a further Regge graviton vertex is introduced in all possible ways, as in Fig 9(b) for the upper-left corner. In the limit $|\mathbf{q}| = \hbar\omega \ll E$ —that we assume throughout the paper—the dominant contributions are for $|\mathbf{q}| \ll |\mathbf{q}'| \sim m_p$, so that no insertions on the \mathbf{q}' -exchange should be considered. As a consequence, for \mathbf{q} in jet 1 and using the CCV gauge [15] in which jet 2 is switched off, only the upper-left and upper-right insertions will be considered.

Consider first the upper-left diagram [Fig. 9(b)] at the imaginary part level. For any fixed values of \mathbf{q} , \mathbf{q}' , and \mathbf{Q} , the integrand has the form

$$\sqrt{\alpha_G} R \int d^2 \mathbf{q}_s e^{i\mathbf{Q}\cdot\mathbf{b}} \left(\frac{1}{q'^2} \right)^2 F^{(\lambda')}(\mathbf{q}'_s + \mathbf{q}', \mathbf{q}'_s) F^{(\lambda')}(\mathbf{q}_s + \mathbf{q}', \mathbf{q}_s) \\ \times \kappa \frac{|q_s|^2}{|q|^2} \left(1 - \frac{q_s^* q_s - q}{q_s q_s^* - q^*} \right) + \dots, \quad (3.19)$$

where $\mathbf{q}_s \equiv \mathbf{q}_2 - \mathbf{q}'$, $\mathbf{q}'_s = \mathbf{q}_s - \mathbf{Q}$, and we have taken, for definiteness, $\lambda = -2$. The $|q_s|^2$ factor in the numerator is needed in order to have the proper counting of $|q_i|^2$ denominators in multi-Regge factorization [29].

We then apply to Eq. (3.19) the same reasoning used in Sec. II B to match the soft and Regge limits. By the approximate identity

$$\frac{|q_s|^2}{|q|^2} \left(1 - \frac{q_s^* q_s - q}{q_s q_s^* - q^*} \right) \\ \simeq \frac{q q_s^* - q^* q_s}{q} \left[\frac{1}{q^* - \frac{\hbar\omega}{E} q_s^*} - \frac{1}{q^* - q_s^*} \right], \quad (3.20)$$

valid in the region $(\hbar\omega/E)|q_s| \ll |q|$, we derive the relationship between Regge and soft insertion analogous to Eqs. (2.13) and (2.25),

$$\text{Regge}|_E = \text{soft}|_E - \text{soft}|_{\hbar\omega}, \quad (3.21)$$

in which

$$\text{soft}|_E = \frac{\hbar\omega}{E} [e^{2i(\phi_{\mathbf{q}} - \frac{\hbar\omega}{E} \phi_{\mathbf{q}_s} - \phi_{\mathbf{q}})} - 1] \quad (3.22)$$

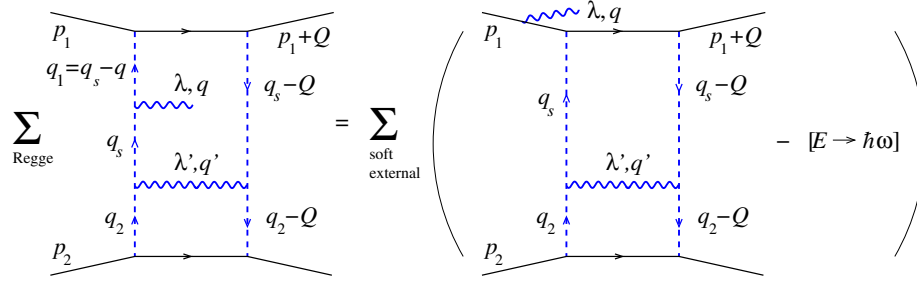


FIG. 10. Diagrammatic representation of the soft-based emission amplitude.

for the upper-left case. A similar relationship holds for the upper-right case and, by including both jets, for any soft insertions, as pictured in Fig. 10.

We note at this point that in Eq. (3.21), the insertion factor for the intermediate particle $p_1 + q_s$ cancels out between left and right insertions, so that we get in total the insertion factor for external legs only, in the form

$$\begin{aligned} & \kappa \left[\frac{E}{\hbar\omega} \left(\frac{q^*}{q} \frac{q - \frac{\hbar\omega}{E} Q}{q^* - \frac{\hbar\omega}{E} Q^*} - 1 \right) - \{E \rightarrow \hbar\omega\} \right] \\ &= \kappa \left[\frac{E}{\hbar\omega} \left(e^{2i(\phi_q - \frac{\hbar\omega}{E} Q - \phi_q)} - 1 \right) - (e^{2i(\phi_{q-Q} - \phi_q)} - 1) \right]. \end{aligned} \quad (3.23)$$

The latter replaces in Eq. (3.19) the sum of Regge insertions and is only dependent on the overall momentum transfer Q (Fig. 10).

Since the above factorization in Q -space holds for any fixed values of Q and $|q'| > |q|$, it is presumably valid for the IR regularization procedure of Eq. (3.18) also, because the latter consists in subtracting the IR singularity due to lower-order eikonal contributions to the S -matrix exponential. We shall then assume Eq. (3.23) for the full graviton emission amplitude associated to H-diagram exchange. This leads to the expression

$$\begin{aligned} \mathcal{M}_H(\mathbf{b}, E, \mathbf{q}) &= \sqrt{\alpha_G} \frac{R}{\pi} \int \frac{d^2 Q}{2\pi} \tilde{\Delta}_H(\mathbf{Q}) e^{iQ \cdot \mathbf{b}} \\ &\times \left[\frac{E}{\hbar\omega} \left(e^{2i(\phi_q - \frac{\hbar\omega}{E} Q - \phi_q)} - 1 \right) \right. \\ &\left. - (e^{2i(\phi_{q-Q} - \phi_q)} - 1) \right], \end{aligned} \quad (3.24)$$

where $\alpha_G \tilde{\Delta}_H(\mathbf{Q})$ is the (regularized) inverse Fourier transform of $\mathfrak{H}\delta_2(b)$ in Eq. (3.18).

The main achievement of Eq. (3.24) is its independence of the detailed structure of the H diagram because of the factorization of the soft insertions in Q -space. Therefore, it is the generalization of the soft-based representation of the unified amplitude to the next-to-leading eikonal exchange.

C. Soft-based representation and eikonal resummation

We have just argued that the single-graviton emission amplitude associated to H-diagram exchange is provided by Eq. (3.24) which is directly expressible in terms of the H-diagram amplitude in Q -space. We can even use the z -representation for the phase transfers

$$e^{2i\phi_\theta} - e^{2i\phi_{\theta'}} = -2 \int \frac{d^2 z}{2\pi z^{*2}} (e^{iAz \cdot \theta} - e^{iAz \cdot \theta'}), \quad (A \in \mathbb{R}^*), \quad (3.25)$$

and by exchanging the order of Q - and z -integrals, we recast Eq. (3.24) in the form

$$\begin{aligned} \mathcal{M} &= \sqrt{\alpha_G} \frac{R}{\pi} e^{-2i\phi_\theta} \int \frac{d^2 z}{2\pi z^{*2}} e^{ibz \cdot \mathbf{q}} \\ &\times \left\{ \frac{E}{\hbar\omega} \left[\Delta \left(\mathbf{b} - \frac{\hbar\omega}{E} bz \right) - \Delta(\mathbf{b}) \right] \right. \\ &\left. - [\Delta(\mathbf{b} - bz) - \Delta(\mathbf{b})] \right\}, \end{aligned} \quad (3.26)$$

where $\Delta = \Delta_0 + \Delta_H$ and $\Delta_H(\mathbf{b}) = R^2/2b^2$, thus generalizing the soft-based representation of Eq. (2.13) to the next-to-leading (NL) term. We shall base on Eq. (3.26) the subsequent formulation of our radiation model.

We note immediately, however, that Eq. (3.26) has a purely formal meaning in the region $|bz - \mathbf{b}| = \mathcal{O}(R)$, because the H-diagram expression (3.18) breaks down whenever R/b is not small. We are thus led to think that we have to know something about the behavior of $\Delta(\mathbf{b})$ in the large-angle regime $b \sim R$ before even writing the representation (3.26) we argued for.

That is precisely what the reduced-action model— as summarized in Sec. III A— provides for us. Indeed, it consists in the resummation of the multi-H diagrams (Fig. 8) of the eikonal, which is the set of two-body irreducible diagrams without a rescattering subgraph. Such diagrams are expected to share with the NL term the property that the central subgraphs have energetic q' -type exchanges, where $|q'|$ is of the order of the Planck mass or

larger, thus suppressing their contribution to soft insertions with $\omega \sim R^{-1} \sim m_p^2/E$.

For that reason, we think we can repeat the argument with peripheral Regge insertions elaborated before and then use the soft-Regge identities (3.21) to derive the external-particles insertion formula (3.24) and the soft-based representation (3.26). As a result, we are now able to look at the integrals in Eq. (3.26) in a realistic way by setting

$$2\Delta(\mathbf{b}) = \frac{2\delta(\mathbf{b})}{\alpha_G} = -2\chi_b + 1 - \frac{1}{t_b}, \quad (3.27)$$

where $\delta(\mathbf{b})$ is the irreducible eikonal function with ACV resummation (after factorization of the IR part $\sim \log L/b$), which extrapolates the NL behavior to small values of $b \sim R$. The latter is given in terms of the solution (3.8) for the reduced-action model action, and $t_b = \tanh \chi_b$ and χ_b are determined by the matching condition of Eq. (3.7).

The expressions (3.27) and (3.8) are now well defined for $b^2 > b_c^2 = \frac{3\sqrt{3}}{2}R^2$, where the role of the singularity at $b = b_c$ will be discussed soon. The result (3.26) contains the resummed modulating function

$$\begin{aligned} \Phi_R(\omega, \mathbf{z}) &\equiv \frac{E}{\hbar\omega} \left[\Delta \left(\mathbf{b} - \frac{\hbar\omega}{E} \mathbf{bz} \right) - \Delta(\mathbf{b}) \right] \\ &\quad - [\Delta(\mathbf{b} - \mathbf{bz}) - \Delta(\mathbf{b})] \\ &\stackrel{\hbar\omega \ll E}{\simeq} -b\Delta'(\mathbf{b}) \hat{\mathbf{b}} \cdot \mathbf{z} + \Delta(\mathbf{b}) \\ &\quad - \Delta(\mathbf{b} - \mathbf{bz}) \equiv \Phi_{R,cl}(\mathbf{z}) \end{aligned} \quad (3.28)$$

[yielding Φ_{cl} of Eq. (2.15) in the classical limit and the large- b region], which generalizes the expressions (2.14) and (2.23) for the leading term and enters the corresponding soft field

$$h_s^{(\lambda)}(\omega, \mathbf{z}) \equiv -\frac{\Phi_R(\omega, \mathbf{z})}{\pi^2 |z|^2 e^{i\lambda\phi_z}}. \quad (3.29)$$

The next step is to sum up all single-graviton emission amplitudes from any of the $\langle n \rangle \sim \alpha_G \gg 1$ irreducible eikonal exchanges with ACV resummation, by taking into account two important effects: (a) the correct phase and \mathbf{q} -dependence for all various incidence angles and (b) the rescattering of the emitted graviton with the fast particles themselves.

Both effects can be taken into account by the generalized \mathbf{b} -space factorization formula explained in Sec. II C for the leading graviton exchange. By replacing $\mathcal{M}_{el} = 2\delta_0$ by 2δ , the resummed soft field of Eq. (2.21) becomes

$$\begin{aligned} &\frac{1}{z^{*2}} \Phi_R(\omega, \mathbf{z}) \frac{e^{2i\delta(\mathbf{b} - \frac{\hbar\omega}{E}\mathbf{bz})} - e^{2i[\delta(\mathbf{b}) + \frac{\hbar\omega}{E}(\delta(\mathbf{b} - \mathbf{bz}) - \delta(\mathbf{b}))]}}{2i[\delta(\mathbf{b} - \frac{\hbar\omega}{E}\mathbf{bz}) - \delta(\mathbf{b}) - \frac{\hbar\omega}{E}(\delta(\mathbf{b} - \mathbf{bz}) - \delta(\mathbf{b}))]} \\ &= \frac{1}{z^{*2}} \frac{e^{2i\delta(\mathbf{b})}}{2i\omega R} [e^{2i\omega R \frac{E}{\hbar\omega} [\Delta(\mathbf{b} - \frac{\hbar\omega}{E}\mathbf{bz}) - \Delta(\mathbf{b})]} - e^{2i\omega R [\Delta(\mathbf{b} - \mathbf{bz}) - \Delta(\mathbf{b})]}], \end{aligned} \quad (3.30)$$

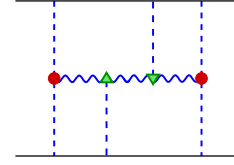


FIG. 11. The first rescattering diagram contributing to the eikonal phase.

where we have canceled out the Φ_R -function at the numerator with the same factor in the denominator and factored out the eikonal S -matrix $e^{2i\delta(\mathbf{b})}$.

By applying the definition (2.24), the full graviton emission probability amplitude becomes

$$\begin{aligned} \frac{\mathfrak{M}_\lambda(\mathbf{b}; \omega, \boldsymbol{\theta})}{e^{i\lambda\phi_\theta}} &= \sqrt{\alpha_G} \frac{R}{\pi} \int \frac{d^2z}{2\pi|z|^2} \frac{e^{ibz \cdot \mathbf{q}}}{2i\omega R} \\ &\quad \times \{ e^{2i\omega R [\Delta(\mathbf{b} - \mathbf{bz}) - \Delta(\mathbf{b})]} - e^{2i\omega R \frac{E}{\hbar\omega} [\Delta(\mathbf{b} - \frac{\hbar\omega}{E}\mathbf{bz}) - \Delta(\mathbf{b})]} \} \\ &\simeq \sqrt{\alpha_G} \frac{R}{\pi} \int \frac{d^2z}{2\pi|z|^2} \frac{e^{ib\omega z \cdot (\boldsymbol{\theta} - \boldsymbol{\Theta}_s)}}{2i\omega R} \\ &\quad \times (e^{-2i\omega R \Phi_{R,cl}(\mathbf{z})} - 1), \end{aligned} \quad (3.31)$$

where $\boldsymbol{\Theta}_s(\mathbf{b}) \equiv -b\Delta'(\mathbf{b})\boldsymbol{\Theta}_E = \boldsymbol{\Theta}_E/t_b$, $\boldsymbol{\Theta}_E \equiv -(2R/b)\hat{\mathbf{b}}$, and $\Phi_{R,cl}$ is the classical limit of Φ_R introduced in Eq. (3.28).

We note that the ωR -dependent correction factor to naive \mathbf{b} -factorization takes into account in a simple and elegant way both the incidence-angle dependence and elastic rescattering with the incident particles including ACV resummation, too.

One may wonder at this point about the role of the rescattering contributions to the irreducible eikonal not included here in $\delta(\mathbf{b})$ and starting at order R^4/b^4 (Fig. 11). The latter presumably have a massless three-body discontinuity and have thus the interpretation of $2 \rightarrow 3 \rightarrow 2$ transition in the rescattering process, leading to a recombination in a two-body state. This would imply taking into account inelastic higher-order contributions to rescattering, a feature which is outside the scope of the present paper.

D. Coherent state and correlation effects

The derivation of the coherent-state operator proceeds now as in Sec. II D if we stick to the ‘‘linear’’ approximation, which neglects correlation effects. The only difference is the replacement of $\delta_0(b)$ by $\alpha_G \Delta(\mathbf{b})$ in the amplitude $\mathfrak{M}_\lambda(\mathbf{b}, \vec{q})$ of Eq. (3.31), so that we obtain

$$\hat{S} = e^{2i\delta(\mathbf{b})} \exp \left\{ \int \frac{d^3q}{\sqrt{2\omega}} 2i \left(\sum_\lambda \mathfrak{M}_\lambda(\mathbf{b}, \vec{q}) a_\lambda^\dagger(\vec{q}) + \text{H.c.} \right) \right\}. \quad (3.32)$$

We shall base on Eq. (3.32) most of the subsequent results. But we want to provide a preliminary discussion of

the limits of that approximation and of the size of correlations that we can envisage. That is important for the ACV-resummed model, because we would like to describe sizeable scattering angles $\Theta_s \sim R/b \sim \mathcal{O}(1)$, while approaching the collapse regime.

We start noticing that many-body correlations are already present from the start in the many-graviton states of Sec. II D and are in principle calculable. For instance, the two-body correlation can be estimated from Eq. (2.29) and is, order of magnitude like,

$$c_{12} = \mathfrak{M}_1 \mathfrak{M}_2(|z_1| \omega_1 R |z_2| \omega_2 R) / \alpha_G. \quad (3.33)$$

We note also that the factors $|z_i| = |x_i/b| \sim 1/\sqrt{\omega_i R}$ are small in the dominant integration region for radiation (Sec. II E), so that c_{12} becomes of relative order $\sqrt{\omega_1 \omega_2}/E \simeq 1/\alpha_G \ll 1$ for $\omega_i R \sim \mathcal{O}(1)$. This means that, within our assumptions, we can neglect finite-order correlations.

One may wonder, however, whether correlated emission can be enhanced by multiplicity effects—not only those of the exchanged gravitons ($\langle n \rangle \sim \alpha_G$) but also those of the emitted ones ($\langle N \rangle \sim \alpha_G \Theta_s^2$), a number which may be large, and even more for $\Theta_s = \mathcal{O}(1)$.

One such effect is certainly present and is due to energy conservation. Even if energy transfer is explicitly considered in the treatment of rescattering in Secs. II C and II D, the kinematical constraints are not explicitly enforced. But such constraints are needed, because the expected average emitted energy $\langle \omega \rangle \equiv E/\langle N \rangle = R^{-1} \Theta_s^{-2}$ is of the order of the so-called classical cutoff [13, 19] and cannot be large if Θ_s increases up to $\mathcal{O}(1)$. This means that the larger values of ωR can be reached only for a smaller number of gravitons, thus distorting the calculation of inclusive distributions. That effect is therefore important but can be included in the coherent state (3.32) and will be discussed in Sec. IV C.

Another kind of multiplicity effect—not included in (3.32)—comes from multigraviton emission by a single exchange. A simple model for that is to consider soft emission which, according to Ref. [7], Sec. IV, is described by the operator eikonal

$$\begin{aligned} \hat{\delta}_{\text{soft}}(\mathbf{b}, a_q) &= \alpha_G \int \frac{d^2 \mathbf{q}_s}{(2\pi)^2} \frac{e^{i\mathbf{q}_s \cdot \mathbf{b}}}{q_s^2} \mathcal{U}_{\text{soft}}^{q_s}(a_q) \\ \mathcal{U}_{\text{soft}}^{q_s}(a_q) &\equiv \exp \left\{ 2\sqrt{G} \int \frac{d^3 q}{\sqrt{2\omega_q}} |\mathbf{q}_s| \right. \\ &\quad \left. \times \frac{\sin(\phi_q - \phi_{q_s})}{|\mathbf{q}|b} [a_\lambda^\dagger(\mathbf{q}) - a_\lambda(\mathbf{q})] \right\}. \end{aligned} \quad (3.34)$$

Here, we can see the nonlinear structure of the operator (3.34) as a “coherent state of coherent states” in the soft limit. Its linear part agrees with the state (3.32) by the approximate form of

$$\mathfrak{M} \simeq \sqrt{\alpha_G} \frac{\Theta_E \sin(\phi_q - \phi_{q_s})}{2\pi |\mathbf{q}|} J_0(|\mathbf{q}|b), \quad (3.35)$$

which is valid in the region $(E/\hbar\omega)|\mathbf{q}| \gg |\mathbf{q}_s| \gg |\mathbf{q}|$ [19]. On the other hand, nonlinear effects in (3.34) are pretty small, because the exchanged graviton coupling α_G affects only the \mathbf{q}_s -dependence and not the \mathbf{q} -dependence. Therefore, the single-exchange multiplicity $\langle N_1 \rangle \sim \langle N \rangle / \alpha_G \sim \mathcal{O}(\Theta_s^2)$ is down by a factor α_G and yields a quite limited enhancement, if any. By comparison, the nontrivial feature of the state (3.32) is that, though being confined to one emitted graviton per exchange, it takes into account all exchanged gravitons' multiplicities and thus produces a reliable ωR dependence.

To conclude, we stick in the following to the linear coherent state (3.32) to describe the main radiation features, but we introduce energy-conservation constraints also, to better understand the large- ωR part when approaching the collapse regime.

IV. FINITE-ANGLE RADIATION AND APPROACH-TO-COLLAPSE REGIME

A. Emission amplitude in the sizeable angle region

In the following, we concentrate on the analysis of the amplitude (3.31) in the semihard frequency region $\omega R \gtrsim 1$, because the very soft gravitons ($\omega \ll b^{-1}$) are already well described by the approach of Sec. II.

In that region, the behavior of (3.31) is quite sensitive to the angular parameter $\Theta_E \equiv 2R/b$, which occurs in the amplitude in two ways: in the overall coupling $\Theta_E \sqrt{\alpha_G}$ and in the explicit expression for the action, which is actually most sensitive, because of the $b = b_c$ branch cut (Sec. III A). Note also the occurrence in the amplitude of $\Delta(\mathbf{b} - \mathbf{bz})$, which may be in the nonperturbative regime in the integration region $|\mathbf{b} - \mathbf{bz}| \lesssim R$ in which its S -matrix factor may be exponentially suppressed as in Eq. (3.11).

For the above reason, we shall cut off the rescattering contributions by the requirement $|\mathbf{b} - \mathbf{bz}| > b_c$. If $\Delta(\mathbf{b})$ is in the perturbative regime $\Theta_E \ll 1$, that change is subleading by a relative power of R^2/b^2 , because of phase-space considerations, and the approach remains perturbative. If instead $0 < (b - b_c)/b \ll 1$, the cutoff procedure can be extended to virtual corrections, by unitarizing the coherent-state operator, as usual, but our approach becomes nonperturbative. Finally, we shall not discuss at all—in this paper—the subcritical case $b \leq b_c$ by limiting ourselves to the $b \rightarrow b_c^+$ approach-to-collapse regime. Considering $b < b_c$ would raise a variety of physical effects at both the elastic and inelastic levels that deserve a separate investigation.

Since we limit ourselves to the $b \geq b_c$ case, we do not expect real problems with S -matrix unitarity, because the tunneling suppression of the elastic channel in Eq. (3.11) is absent. Nevertheless, the associated radiation shows quite

interesting features, especially in the approach-to-collapse regime $b \rightarrow b_c^+$, that will be illustrated in the following.

Starting from the energy emission distribution of type (2.40)

$$\frac{dE^{\text{GW}}}{d\omega} = 2G_s \frac{\Theta_E^2}{\pi^2} \int \frac{d^2z}{|z|^4} \left(\frac{\sin \omega R \Phi_{\text{R,cl}}(z)}{\omega R} \right)^2 \quad (\omega R \gtrsim 1), \quad (4.1)$$

we shall therefore distinguish two cases, in the large ωR region:

- (a) $\omega R \gg (1 - \frac{b_c^2}{b^2})^{-3/2} \equiv (2\beta)^{-3/2}$: That is the truly small-angle regime, far away from the critical region $1 - \frac{b_c^2}{b^2} \rightarrow 0$, or not too close to it. In that case, ωR is very large, which means very small z 's [$|y|^2 \approx |x|^2/\sqrt{\beta} \approx \mathcal{O}(1/\omega R)$], so that the qualitative features of the radiation can be derived from the small- z approximation of the modulating function

$$\Phi_{\text{R,cl}} \approx -\frac{1}{2} [D_2(b)x^2 - D_1(b)y^2] + \mathcal{O}(|z|^3), \quad (4.2)$$

where we have used the expansion

$$\begin{aligned} \Phi_{\text{R,cl}} &= \Delta(b) - \Delta(|\mathbf{b} - b\mathbf{z}|) - \Delta'(b)\mathbf{b} \cdot \mathbf{z} \quad (4.3a) \\ &\approx -\frac{1}{2} \frac{\partial^2 \Delta}{\partial b_i \partial b_j} b^2 z_i z_j \\ &= \frac{1}{2} [-\Delta''(b) b^2 \hat{b}_i \hat{b}_j - b \Delta'(b) (\delta_{ij} - \hat{b}_i \hat{b}_j)] \end{aligned} \quad (4.3b)$$

yielding [by use of Eqs. (3.7) and (3.8)]

$$D_1 = -b \Delta'(b) = \frac{1}{t_b}, \quad D_2 = b^2 \Delta''(b) = \frac{1 + t_b^2}{t_b (3t_b^2 - 1)}. \quad (4.4)$$

Here, we note that $D_1 \approx D_2 \approx 1$ for $b \gg b_c$, thus recovering Eq. (2.45) discussed before, while $D_1 \approx \sqrt{3}$, $D_2 \approx \sqrt{2}(1 - \frac{b_c^2}{b^2})^{-1/2}$ for $\beta \ll 1$ [Eq. (3.12)], and thus D_2 diverges for $\beta \rightarrow 0$. Correspondingly, we get a formula similar to (2.40),

$$\frac{dE_{\text{cl}}^{\text{GW}}}{d\omega} = 2G_s \frac{\Theta_E^2}{\pi} \int \frac{d^2z}{\pi|z|^4} \left[\frac{\sin(\frac{\omega R}{2}(D_2 x^2 - D_1 y^2))}{\omega R} \right]^2, \quad (4.5)$$

where, however, we should assume $|x|^2/\sqrt{\beta} \ll |x|^{3/2}$ (or $|x| \ll \beta$) whenever $\beta \ll 1$, because the actual behavior of $\Delta(\mathbf{b} - b\mathbf{z})$ is that of a branch cut with index $3/2$, with a small convergence radius in the x -variable. We should therefore require $\omega R \gg \beta^{-3/2} \gg 1$, as stated, so that such a regime actually disappears in the limit $\beta \rightarrow 0$.

- (b) $1 \ll \omega R \ll \beta^{-3/2}$: That region opens up in the critical regime $0 < \beta \ll 1$ and is dominant for $\beta \rightarrow 0$. However, the quadratic small- z expansion is no longer valid in the x -variable (because of the divergent coefficient), and the dominant approximation in the $|y| \approx |x| \ll 1$ region becomes of the type

$$\begin{aligned} -\Phi_{\text{R,cl}}(z) &\approx -\Phi_1(x) \\ &\equiv 4 \left[\frac{1}{3} (\beta - x)^{3/2} - \frac{1}{3} \beta^{3/2} + \frac{1}{2} x \sqrt{\beta} \right] \\ &\stackrel{|x| \ll \beta}{\approx} \frac{x^2}{2\sqrt{\beta}}, \end{aligned} \quad (4.6)$$

where we have neglected, for simplicity, the y -dependence. We thus obtain what we shall call the one-dimensional approximation to Φ_{R} , which is easily derived by expanding all terms in the expression (3.28) of $\Phi_{\text{R,cl}}$ for $0 < \beta \ll 1$, both in β and in z and making the $(b - b_c)^{3/2}$ behavior explicit by Eq. (3.12).

The striking feature of (4.6) is that, in the $\beta \ll |x| \ll 1$ region, the dominant small- x behavior is $\Phi_1 \approx (4/3)|x|^{3/2}$, reflecting the branch cut of the ACV-resummed action, which is responsible for the very large second derivative (large tidal force) in (4.3b). By inserting that behavior in (4.1), the corresponding distribution becomes

$$\begin{aligned} \frac{1}{\sqrt{s}} \frac{dE^{\text{GW}}}{d\omega} \Big|_{\text{enhanced}} &= \frac{\Theta_c^2}{\pi\omega} \left(\frac{\omega R}{3} \right)^{1/3} \Gamma(2/3), \\ \Theta_c^2 &\equiv \Theta_E^2(b_c) = \frac{8}{3\sqrt{3}} \end{aligned} \quad (4.7)$$

and falls off as $(\omega R)^{-2/3}$ only. That radiation enhancement is a direct consequence of the critical index $3/2$ of the action branch cut at $b = b_c$.

We thus realize that, with increasing R/b , we quit the small-angle, weak-coupling regime a, in which the radiated-energy fraction is small (of order Θ_E^2) and shows at most a $\log(\omega_M R)$ dependence with an upper frequency cutoff ω_M , and we enter the strong-coupling regime b, in which such a fraction increases like $\Theta_E^2(\omega_M R)^{1/3}$, thus endangering the energy-conservation bound.

The possible violation of energy conservation—which is nevertheless taken into account at the linear level in the ω 's for rescattering—is related to the fact that the kinematical constraints are not explicitly incorporated in multigraviton production amplitudes and that multiparticle correlations are neglected, also. We shall introduce such constraints in Sec. IV C.

B. Radiation enhancement and scaling

1. Small- z radiation spectrum

In this section, we present plots of the resummed amplitude and of the corresponding radiated-energy

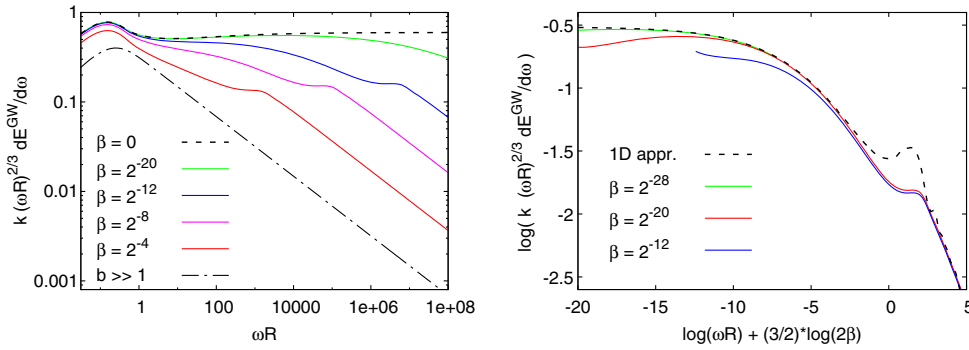


FIG. 12. Left: the resummed spectrum for $\omega R \gtrsim 1$ in the approach-to-collapse regime $b \rightarrow b_c$ ($\beta \rightarrow 0$) for various values of β ranging from $1/2$ ($b \rightarrow \infty$) to 0 ($b \rightarrow b_c$). The spectrum has been multiplied by $(\omega R)^{2/3}$ in order to highlight the enhancement in the intermediate regime $1 \ll \omega R \ll \beta^{-3/2}$, followed by the asymptotic $1/\omega$ falloff. Right: some curves have been shifted horizontally and somewhat magnified in the neighborhood of the transition region, showing the scaling behavior with respect to the variable $a = (4\beta)^{3/2}\omega R$; the black-dashed curve represents the one-dimensional approximate representation (4.8). As usual, spectra are reduced by the factor $k = (Gs\Theta_E^2)^{-1}$.

distribution obtained by numerical evaluation. In this way, we confirm the asymptotic behaviors derived in Sec. IV A and visualize the shape of such quantities in the transition regions.

Let us start by displaying the main features of the gravitational wave spectrum obtained with the ACV resummation in the classical limit $\hbar\omega \ll E$ but close to the collapse region $b \gtrsim b_c$. For $\omega R \gtrsim 1$, this is obtained by substituting the reduced-action model field (3.28) [actually, its classical limit $\Phi_{R,cl}$ of Eq. (4.3a)] in place of its leading counterpart Φ inside Eq. (2.40). The results for various values of β are shown in Fig. 12. According to the estimates in Sec. IV A, at smaller and smaller $\beta \ll 1$, there is a larger and larger intermediate region $1 \ll \omega R \ll \beta^{-3/2}$ of a reduced decrease of the frequency spectrum $\sim \omega^{-2/3}$, followed by the typical asymptotic ω^{-1} falloff at $\omega R \gg \beta^{-3/2}$. In order to better discriminate between the two regimes, the spectrum has been multiplied by $(\omega R)^{2/3}$, so that in the intermediate enhanced region, the curves are almost flat.

In the first plot of Fig. 12, the black dotted-dashed curve ($\beta = 1/2$) represents the small-angle spectrum described in Sec. II E. Decreasing the value of β , we obtain the solid curves (red, magenta, blue, and green), and we observe the expected enhancement that amounts to a numerical factor of order 1 for $\omega R \lesssim 1$ but becomes much more important for large $\omega R \gtrsim 1$. It is also clear that the extension of the enhanced regime increases while decreasing β . In the limit $\beta \rightarrow 0$, the rescaled spectrum approaches the almost horizontal dashed line.

It is apparent that the shapes of the curves are quite similar at large ωR , including the transition region between the enhanced and asymptotic regimes. By rescaling the independent variable $\omega R \rightarrow \omega R \beta^{3/2}$, the curves at small β go on top of each other, as shown in the right plot of Fig. 12. In other words, the asymptotic shape of the spectrum is a function of

the single variable $a \equiv (4\beta)^{3/2}\omega R$. This scaling property can be understood by exploiting the small- z expansion (4.6) that, substituted into Eq. (2.40), provides the approximate representation

$$\begin{aligned} & \frac{1}{Gs\Theta_E^2} (\omega R)^{2/3} \frac{dE}{d\omega} \\ & \simeq \frac{2}{\pi} a^{-1/3} \int_{-1}^{\infty} dt \frac{\sin\{a[\frac{1}{3}((1+t)^{3/2}-1) - \frac{t}{2}]\}}{|t|(1+\sqrt{1+t})} \xrightarrow{a \rightarrow 0} \frac{2\Gamma(2/3)}{3^{1/3}\pi} \\ & a \equiv (4\beta)^{3/2}\omega R, \end{aligned} \quad (4.8)$$

which depends only on the scaling variable a . This function is displayed in the black dashed line on the right plot of Fig. 12, and it describes well the scaling behavior in the enhanced region $a \ll 1$ and reasonably well the large- ωR region $a \gg 1$.

2. Angular behavior

The angular behavior of graviton radiation associated to large scattering angles $\Theta_s \sim 1$ can be obtained by numerical integration of the amplitude (3.31). However, in the main region of the spectrum, namely $\omega R \gtrsim 1$, it can be more conveniently described by using the small- z approximation (4.2) of the modulating function $\Phi_{R,cl}$. The main point here is that the two dispersion coefficients D_1 and D_2 , which are equal for the small scattering angle, become more and more different when approaching the critical angle Θ_c . This fact causes the ensuing distribution of graviton radiation to be more and more directional, still concentrated at $\theta \approx \Theta_s$, but with a larger dispersion, in particular along the x -direction, i.e., that of the scattering plane. This is clearly seen in Fig. 13, where we compare on the $A \equiv \sqrt{\omega R} \frac{\theta - \Theta_s}{|\Theta_s|}$ plane the “isotropic” radiation (a) when $D_1 = D_2 = 1$ with the

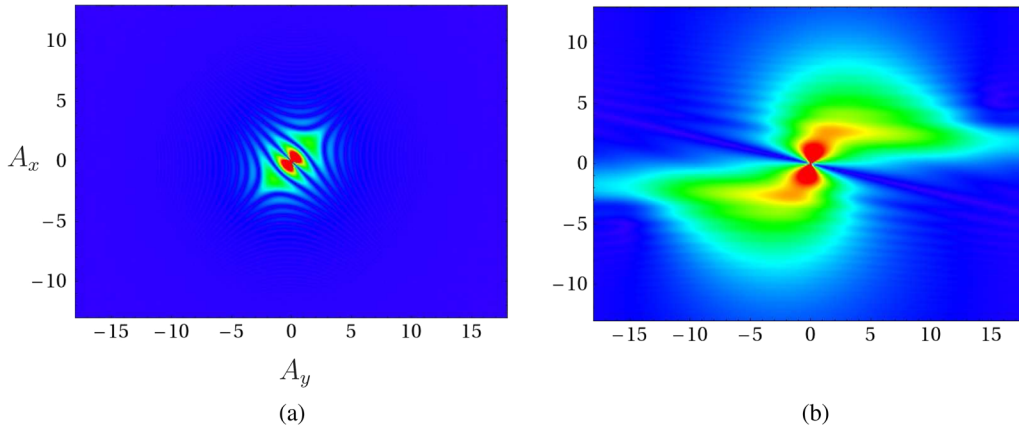


FIG. 13. Emission pattern of gravitational radiation for $\lambda = -2$ on the tangent space centered at Θ_s , parametrized by $A \equiv \sqrt{\omega R} \frac{\theta - \Theta_s}{|\Theta_s|}$. (a) the isotropic case $D_1 = D_2$ discussed in Sec. II E; (b) anisotropic case with $D_1 = \sqrt{3}$, $D_2 = 32$.

“anisotropic” case (b) $D_1 = \sqrt{3}$, $D_2 = 32$ (corresponding to $\beta \approx 0.001$).

We see, first of all, that in the collapse region [Fig. 13(b)], the radiation is strongly enhanced, still keeping its correlation with the outgoing particle 1’ in the overall picture of the two jets. Furthermore, the larger dispersion in θ_x compared to θ_y , gives a rationale for the one-dimensional approximation (4.8) in the conjugated variables x and y . Finally, such features are valid for any given frequency range $\Delta\omega$ and are thus somewhat independent of their relative normalization, which is possibly affected by energy-conservation constraints, to be discussed next.

C. Energy conservation and temperature

In order to take into account energy-conservation constraints, we shall calculate coherent-state amplitudes and distributions by setting—event by event—the explicit energy bound $\sum_{i=1}^N \hbar\omega_i < E$, in which we refer to a single “jet,” say along p_1 .³ Such bounds are effectively extended to virtual corrections by a factorization assumption, as proposed by Ref. [23] on the basis of the Abramovsky Gribov Kancheli (AGK) [34] cutting rules (see also Sec. 4.3 of Ref. [5]).

More explicitly, we modify the original independent-particle distributions (2.37) in a radiation sample of energy up to E by introducing the corresponding kinematical bounds together with a rescaling factor $1/N(E)$ in probability [or $1/\sqrt{N(E)}$ in amplitude] to be determined by unitarity. For instance, by considering for simplicity the ω -variables only, we define the energy-conserving distributions

³The point is that the energy of the forward (backward) gravitons is essentially taken at the expenses of the sole particle 1 (2).

$$\begin{aligned} \tilde{P}_0 &= \frac{P_0}{N(E)}, \\ d\tilde{P}(\{\omega_i N_i\}) &= \frac{P_0}{N(E)} \prod_i \frac{[p(\omega_i)\Delta(\omega_i)]^{N_i}}{N_i!} \\ &\times \Theta\left(E - \sum_i \hbar\omega_i N_i\right), \end{aligned} \quad (4.9)$$

where the $p(\omega)$ density is given by (2.38), with the amplitude $\mathfrak{M}_\lambda(\mathbf{b}, \vec{q})$ in (3.31). We have also discretized the Fock space in regions of extension $\Delta(\omega_i)$, containing a number of gravitons N_i each.

The normalization factor $N(E) > 0$ in (4.9) is determined by the unitarity condition $\sum_{\{N_i\}} \tilde{P}(\{N_i\}) = 1$ and takes the form [cf. Eq. (2.37)]

$$N(E) = \int_{-\infty}^{+\infty} \frac{d\lambda}{2\pi i} \frac{e^{\lambda E}}{\lambda + \varepsilon} \exp\left\{\int_0^\infty d\omega p(\omega)[e^{-\omega\lambda} - 1]\right\}, \quad (4.10)$$

which carries the energy-conservation constraints and is obtained by summing over all events the (positive) partial probabilities. We stress the point that E in Eq. (4.10) is the energy available for the measures being considered, so that $E = \sqrt{s}/2$ if we consider the whole jet, but becomes $\sqrt{s}/2 - \hbar\omega$ if we consider events associated to an observed graviton ω in that jet, and so on. On the basis of Eqs. (4.9) and (4.10), it is straightforward to obtain, for the inclusive distributions,

$$\begin{aligned} \frac{d\mathcal{N}}{d\omega} &= p(\omega) \frac{N(E - \hbar\omega)}{N(E)}, \\ \frac{d^2\mathcal{N}}{d\omega_1 d\omega_2} &= p(\omega_1)p(\omega_2) \frac{N(E - \hbar\omega_1 - \hbar\omega_2)}{N(E)} \end{aligned} \quad (4.11)$$

and so on. We notice also that virtual corrections are explicitly incorporated in (4.10) via the normal ordering of

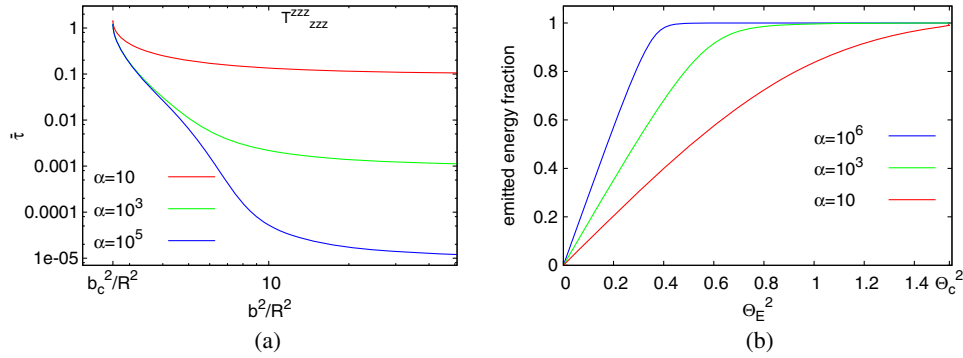


FIG. 14. (a) Dependence of the saddle point $\bar{\tau}$ on the impact parameter b^2 , for various values of α_G ; (b) emitted-energy fraction vs Θ_E^2 for various values of α_G .

the state (3.32) [cf. Eq. (2.36)] and that $N(E)$ is actually infrared safe.

The main point is now that the inclusive distributions (4.11) carry $N(E)$ -dependent correction factors due to the phase-space restrictions $E \rightarrow E - \hbar\omega, \dots$, and so on, that will turn out to suppress the large- ωR region by an exponential cutoff. Arguments for a cutoff are provided also in the approach of Ref. [16] to the trans-Planckian scattering without impact parameter identification of Ref. [14].

In order to estimate $N(E)$, it is convenient to rewrite it in terms of the quantity ($\lambda \equiv R\tau$),

$$\frac{\langle \hbar\omega \rangle_\tau}{\sqrt{s}/2} \equiv F(\tau) = \int_0^\infty d\omega \frac{\hbar\omega}{\sqrt{s}/2} p(\omega) e^{-\omega R\tau}, \quad (4.12)$$

which represents the (exponentially weighted) radiated-energy fraction, given in our case (3.31) by [cf. Eq. (4.1)]

$$F(\tau) = \frac{\Theta_E^2}{\pi^2} \int \frac{d^2z}{|z|^4} \int_0^\infty \frac{\sin^2(\omega R \Phi_{R,cl})}{(\omega R)^2} e^{-\omega R\tau} d(\omega R). \quad (4.13)$$

We then obtain from Eq. (4.10) ($\alpha_G = R\sqrt{s}/2 = Gs$) the expression

$$N(E) = \text{const} \int_{\epsilon-i\infty}^{\epsilon+i\infty} d\tau \exp \left\{ ER\tau - \log \tau - \alpha_G \int_0^\tau F(\tau') d\tau' \right\}, \quad (4.14)$$

and we proceed to estimate it by the saddle-point method. The saddle-point value $\bar{\tau} > 0$ is determined by the equation ($E = \sqrt{s}/2$)

$$F(\bar{\tau}) = 1 - \frac{1}{\alpha_G \bar{\tau}}, \quad (4.15)$$

which represents the share between emitted (lhs) and preserved ($1/\alpha_G \bar{\tau}$) energy fractions at the saddle-point exponent $\bar{\tau}$. Fluctuation corrections are also calculable (Appendix A) and will be discussed shortly.

The numerical evaluation of (4.15) (Fig. 14) is better understood by working out Eq. (4.13) in the form

$$1 - \frac{1}{\alpha_G \bar{\tau}} = F(\bar{\tau}) = \frac{\Theta_E^2}{\pi^2} \int \frac{d^2z}{|z|^4} |\Phi(z)| I\left(\frac{2|\Phi(z)|}{\bar{\tau}}\right), \quad (4.16)$$

where, by explicit integration,

$$\tan \chi I(\tan \chi) = \chi \tan(\chi) + \frac{1}{2} \log(\cos^2 \chi). \quad (4.17)$$

The result shows that $\bar{\tau} \sim \mathcal{O}(1/\alpha_G)$ in the small-angle region ($b \gg R$), while $\bar{\tau} = \mathcal{O}(1)$ in the collapse regime. In between, the radiated-energy fraction varies from 0 to 1.

In order to understand the role of $\bar{\tau}$ for the energy-conservation cutoff, we estimate the inclusive distribution (4.11) at the saddle point, and we find

$$\frac{d\mathcal{N}}{d\omega} = p(\omega) e^{-(\bar{\tau} + \Delta\tau)\omega R}, \quad (4.18)$$

where the $\bar{\tau}$ term in the exponent comes from the explicit energy dependence of $N(E - \omega)$ and the correction $\Delta\tau$ comes from the implicit one through $\bar{\tau}(E - \omega)$, to which—by $\bar{\tau}$ -stationarity—mostly fluctuations contribute. We show in Appendix A that this kind of correction is sizeable when $\bar{\tau} = \mathcal{O}(1/\alpha_G)$ is small (where, however, the cutoff is not really important), while it is small when $\bar{\tau} = \mathcal{O}(1)$ is essential, that is, in the approach-to-collapse regime. The cutoff exponent $\bar{\tau}$ has already been used in the definitions (4.13) and (4.16).

In more detail, it is useful to distinguish a very small-angle regime $\Theta_s^2 \ll \bar{\Theta}^2 \equiv 1/\log \alpha_G$, in which $\bar{\Theta}^2$ acts as threshold for important energy-conservation effects like energy fractions of order 0.5, say [Figs. 14(b) and Eq. (2.42)]. Below it, the radiated fraction $\sim \Theta_s^2$ is very small, and so is $\bar{\tau} \sim 1/\alpha_G$. Furthermore, the exponent $\bar{\tau} + \Delta\tau \sim \Theta_s^2/\alpha_G$ is even smaller than $\bar{\tau}$ because of cancellations with the term $\Delta\tau$ (Appendix A), thus leading to negligible conservation corrections.

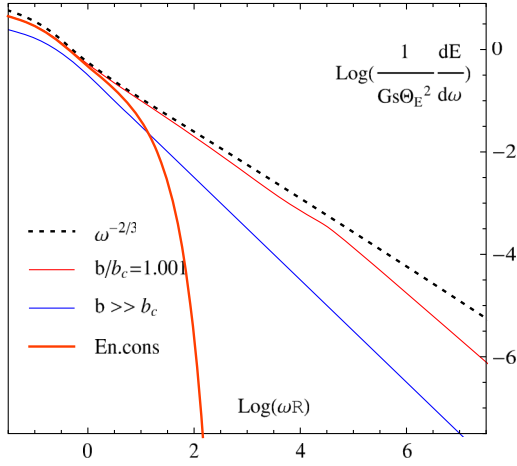


FIG. 15. Frequency spectrum of graviton radiation in various contexts. Three curves have no energy-conservation constraints and correspond to large b/R where subleading effects are negligible (blue), b close to the critical parameter b_c where subleading effects causes the enhancement (thin red), and the limit $b \rightarrow b_c^+$ (dashed black). The last curve (thick red) shows the suppression due to energy-conservation constraints in the case of b close to b_c .

On the other hand, for Θ_s^2 above $\bar{\Theta}^2$, both the exponent part $\bar{\tau}$ and the radiated fraction increase (Fig. 14) up to $\mathcal{O}(1)$ for $\Theta_E^2 \rightarrow \Theta_c^2 = \mathcal{O}(1)$, while $\Delta\tau/\bar{\tau}$ becomes $\mathcal{O}(1/\alpha_G) \ll 1$, that is, small.

In that case—of strong coupling and radiation enhancement—the whole energy is radiated off, and this fact fixes $\bar{\tau} = \tau_c = 1.2$ in a rather precise way. Furthermore, the same exponent (with $\Delta\tau/\bar{\tau} \sim 1/\alpha_G \ll 1$) occurs in all the graviton distributions (4.11) which—because of such approximate universality—turn out to be approximately factorized and thus weakly correlated, even after the inclusion of energy conservation. In other words, while the rescaling factor $\sqrt{N(E)}$ keeps the phase relations of the coherent state (3.32) among the various ω -bins, it also introduces, by the E -dependence of (4.10) and the ω -dependence of (4.11), an almost universal frequency cutoff parameter R^{-1} , a “quasi-temperature” we would say, in the approach-to-collapse regime. Numerically, the exponent $\tau_c R$ turns out to be of the order of the inverse Hawking temperature for a black hole mass $\approx 0.1\sqrt{s}$, notably smaller than \sqrt{s} , and the corresponding spectrum—in each one of the two jets with $E = \sqrt{s}/2$ of which our radiation consists—is given in Fig. 15.

Our semiclassical method does not allow, at present, a precise interpretation of the features just mentioned in terms of black hole physics, mostly because of our ignorance of what a black hole really is in quantum physics. Nevertheless, we think that, applying our soft-based representation to the approach-to-collapse regime, we have constructed a coherent radiation sample which shares some of its properties with a Hawking radiation, thus suggesting a deeper relationship. That fact, because of

coherence, goes in the direction of a quantum theory overcoming the information paradox, even if the details of such a relationship are not known yet.

V. OUTLOOK

The main technical progress presented here is the extension of the semiclassical graviton radiation treatment in trans-Planckian scattering to cover finite scattering angles $\sim R/b$. That result is in turn based on the ACV eikonal resummation and on the validity—for such a reduced-action model—of the soft-based representation of the radiation amplitude argued for in Sec. III.

After such steps, we are really able to follow the approach to the classical collapse regime by a fully explicit, unitary coherent state, given the fact that collapse is signalled by a branch cut singularity of the action at $b = b_c = \mathcal{O}(R)$ with some scattering angle $\Theta_c = \mathcal{O}(1)$ and branch-cut index $3/2$. While b_c and Θ_c are expected to be somewhat model dependent, the index $3/2$ is expected to be robust because it yields the first nonanalytic behavior, by the action stationarity in the angular parameter t_b .

The first striking feature that we notice is that, because of the index $3/2$, the action has very large second derivatives (tidal forces) and thus yields a radiation enhancement causing almost the whole energy be radiated off for $b \rightarrow b_c^+$. Actually, it also requires the enforcement of the kinematical constraints in order to ensure energy conservation.

Energy-conservation constraints (Sec. IV) are introduced in real emission event by event and transferred to virtual corrections in some approximation which amounts to a factorization assumption, natural for the weakly correlated coherent state that we have constructed. The outcome is that energy-conservation effects, which are negligible for $\Theta_s \ll 1$, are instead quite important in the approach-to-collapse regime and provide an exponential suppression of the large- ωR region. The latter is approximately universal; that is, it occurs in all the inclusive distributions, with small corrections and weak correlations, both depending on the parameter $1/\alpha_G$, where $\alpha_G = Gs/\hbar \gg 1$ is the magnitude of the final multiplicity.

The conclusive features just mentioned show that our radiation sample (corresponding to two jets with masses up to $\sqrt{s}/2$)—though coherent by construction—is characterized by an almost universal, exponential frequency cutoff close to $1/R$, which plays a role analogous to the Hawking temperature (at a mass notably smaller than \sqrt{s}). Such a fact suggests a deeper relationship with the possible collapse dynamics, the boundaries of which are, however, difficult to pinpoint, in view of both our approximations and our ignorance about the nature of a quantum black hole. We nevertheless think, because of coherence, that our results go in the direction of a quantum theory overcoming the information paradox, even if details of their relationship to black hole physics are not known yet.

ACKNOWLEDGMENTS

It is a pleasure to thank Gabriele Veneziano for a number of interesting conversations on the topics presented in this paper and Domenico Seminara for useful discussions. We also wish to thank the Galileo Galilei Institute for Theoretical Physics for hospitality while part of this work was being done.

APPENDIX A: FLUCTUATION CORRECTIONS TO INCLUSIVE DISTRIBUTIONS

It is straightforward to introduce a quadratic fluctuation expansion in Eq. (4.14) to yield the normalization factor

$$\begin{aligned}
 N(E) &= \int_{\bar{\tau}-i\infty}^{\bar{\tau}+i\infty} \frac{d\tau}{2\pi i} \exp \left\{ ER\bar{\tau} - \log \bar{\tau} - \alpha_G \int_0^{\bar{\tau}} F(\tau') d\tau' \right. \\
 &\quad \left. + \frac{1}{2} (\tau - \bar{\tau})^2 \left[\frac{1}{\bar{\tau}^2} - \alpha_G F'(\bar{\tau}) \right] \right\} \\
 &\simeq \text{const} \exp \left\{ \left[ER\bar{\tau} - \alpha_G \int_0^{\bar{\tau}} F(\tau') d\tau' \right] \right. \\
 &\quad \left. - \frac{1}{2} \log(1 - \alpha_G \bar{\tau}^2 F'(\bar{\tau})) \right\}. \quad (\text{A1})
 \end{aligned}$$

We note that the $\log \bar{\tau}$ term cancels out, so that the overall size of fluctuations is determined by the function

$$f(\bar{\tau}) \equiv -\alpha_G \bar{\tau}^2 F'(\bar{\tau}) \simeq \begin{cases} \frac{\Theta_E^2}{2\pi} \alpha_G \bar{\tau} & (\Theta_E \ll 1) \\ \frac{1}{3} \alpha_G \bar{\tau}^{2/3} \tau_c^{1/3} & (\Theta_E \simeq \Theta_c). \end{cases} \quad (\text{A2})$$

Although this function is pretty small (large) in the small-(large-)angle regime, its relative importance with respect to the exponent part $\bar{\tau}$ goes just in the opposite. In fact, in the small- $\bar{\tau}$ regime (where the cutoff is unimportant), the expansion of the remaining log term produces contributions of order comparable to those in square brackets.

To better understand this point, we combine Eq. (A1) with the saddle-point equations

$$ER = \alpha_G F(\bar{\tau}) + \frac{1}{\bar{\tau}}, \quad \bar{\tau}'(E) = -R\bar{\tau}^2 \frac{1}{1 + f(\bar{\tau})} \quad (\text{A3})$$

to get, after some algebra,

$$\begin{aligned}
 \frac{d \log N(E - \omega)}{dE} \Big|_{\omega=0} &= R\bar{\tau}(E) + \frac{\partial \log N}{\partial \bar{\tau}} \Big|_{\bar{\tau}(E)} \bar{\tau}'(E) \\
 &= R\bar{\tau}(E) \left[\frac{f(\bar{\tau})}{1 + f(\bar{\tau})} + \frac{\bar{\tau} f'(\bar{\tau})}{2(1 + f(\bar{\tau}))^2} \right] \\
 &= R\bar{\tau} \left(1 + \frac{\bar{\tau}}{2} \frac{\partial}{\partial \bar{\tau}} \right) \left(\frac{f}{1 + f} \right). \quad (\text{A4})
 \end{aligned}$$

Consider first the strong coupling regime in which $\bar{\tau} = \mathcal{O}(1)$. It is clear that $f(\bar{\tau})$ is $\mathcal{O}(\alpha_G)$, so that

$$\frac{d\mathcal{N}}{d\omega} \simeq p(\omega) e^{-\omega R(\bar{\tau} + \Delta\tau)} \simeq p(\omega) e^{-\omega R\bar{\tau}} \quad (\text{A5})$$

with a correction

$$\frac{\Delta\tau}{\bar{\tau}} = \left(1 + \frac{\bar{\tau}}{2} \frac{\partial}{\partial \bar{\tau}} \right) \left(\frac{-1}{1 + f} \right), \quad (\text{A6})$$

which is small, $\Delta\tau/\bar{\tau} = \mathcal{O}(1/\alpha_G)$, leading to an approximately universal exponent $\bar{\tau}$.

On the other hand, in the weak coupling regime, $\Theta_E \ll 1$, $\bar{\tau}$ is small, starting $\mathcal{O}(1/\alpha_G)$, so that $f = \mathcal{O}(\Theta_E^2)$ is small, too. As a consequence, relative corrections are large, so as to allow cancellations with the leading term and an even smaller exponent. That is fortunately unimportant, because energy-conservation corrections are small in that regime. For instance, in the regime $\Theta_E^2 \ll 1$ and $\bar{\tau} = \mathcal{O}(1/\alpha_G)$, we get

$$\bar{\tau} + \Delta\tau \simeq \bar{\tau} \frac{f}{1 + f} = \mathcal{O}(\Theta_E^2/\alpha_G), \quad (\text{A7})$$

yielding negligible corrections to the naive inclusive distribution. We conclude that for $\Theta_E \ll 1$, inclusive distributions avoid the energy-conservation cutoff, while for $\Theta_E \simeq \Theta_c = \mathcal{O}(1)$, such a cutoff is provided by $\bar{\tau}$ and is approximately universal. The final multiplicity is provided by (A5) and is of $\mathcal{O}(\alpha_G)$ with a finite coefficient.

APPENDIX B: ONE-DIMENSIONAL INTEGRAL REPRESENTATION OF THE AMPLITUDE AT LARGE ωR

We want to give a simple representation of the graviton emission amplitude for large $\omega R \gg 1$. According to the discussion in Sec. II E, the emission amplitude \mathfrak{M} is dominated by the small- z region, where the modulation function Φ_R can be approximated by its quadratic expansion (4.2). We can therefore express \mathfrak{M} in terms of the two-dimensional complex integral

$$\begin{aligned}
 I(\mathbf{A}) &= \int \frac{d^2 Z}{2\pi i} \frac{e^{i(ZA^* + Z^*A)}}{Z^{*2}} [e^{i(D_2 x^2 - D_1 y^2)} - 1], \\
 (Z &= x + iy), \quad (\text{B1})
 \end{aligned}$$

as in Eq. (2.45). For the resummed amplitude, we note the presence of the two dispersion coefficients D_1 and D_2 that are different for finite b .

Our aim here then is to provide a simple representation of $I(\mathbf{A})$. Gaussian integration is possible by eliminating the double pole by derivation with respect to A :

$$\begin{aligned}
-\frac{\partial^2}{\partial A^2} I(A, A^*) &= \int \frac{dx dy}{2\pi i} e^{i(2xA_1 + 2yA_2)} [e^{i(D_2 x^2 - D_1 y^2)} - 1] \\
&= \frac{1}{2i\sqrt{D_1 D_2}} e^{-i\frac{A_1^2}{D_2} + i\frac{A_2^2}{D_1}} \\
&= \frac{1}{2i\sqrt{D_1 D_2}} e^{-i\frac{(A+A^*)^2}{4D_2} - i\frac{(A-A^*)^2}{4D_1}} \\
&= \frac{e^{iA^+ A^-}}{2i\sqrt{D_1 D_2}}, \\
A^\pm &\equiv \frac{A_2}{\sqrt{D_1}} \pm \frac{A_1}{\sqrt{D_2}}. \tag{B2}
\end{aligned}$$

The integral can be reconstructed if we knew the boundary conditions.

An alternative method is to perform one of the x, y integrals in (B1) by noticing that the exponent is bilinear in $\xi, \eta \equiv \sqrt{D_2}x \mp \sqrt{D_1}y$, so that one variable ξ or η can be kept fixed and real, while the other is complexified and deformed on the pole. By using

$$\begin{aligned}
x &= \frac{\xi + \eta}{2\sqrt{D_2}}, \\
y &= \frac{\eta - \xi}{2\sqrt{D_1}}, \\
x - iy &= \frac{\xi d + \eta d^*}{2\sqrt{D_1 D_2}}, \\
d &\equiv \sqrt{D_1} + i\sqrt{D_2} = \sqrt{D_1 + D_2} e^{i\chi}, \\
2\mathbf{z} \cdot \mathbf{A} &= A_1 \frac{\xi + \eta}{\sqrt{D_2}} + A_2 \frac{\eta - \xi}{\sqrt{D_1}} \\
&= \xi \left(\frac{A_1}{\sqrt{D_2}} - \frac{A_2}{\sqrt{D_1}} \right) \\
&\quad + \eta \left(\frac{A_1}{\sqrt{D_2}} + \frac{A_2}{\sqrt{D_1}} \right)
\end{aligned}$$

and integrating over η at fixed real ξ at the double pole $\eta = e^{-i2\gamma}\xi$, $\gamma = \pi/2 - \chi$, we obtain (in the case $A^+ > 0$)

$$\begin{aligned}
I &= \int \frac{d\xi d\eta}{4\pi i \sqrt{D_1 D_2}} \frac{e^{i\eta\xi} - 1}{(\xi d + \eta d^*)^2} 4D_1 D_2 e^{i\eta \left(\frac{A_1}{\sqrt{D_2}} + \frac{A_2}{\sqrt{D_1}} \right) + i\xi \left(\frac{A_1}{\sqrt{D_2}} - \frac{A_2}{\sqrt{D_1}} \right)} \\
&= \int_{-\infty}^0 d\xi \frac{2i\sqrt{D_1 D_2}}{d^{*2}} [e^{i\xi e^{-i2\gamma}(\xi + A^+) - i\xi A^-} (\xi + A^+) \Theta(\xi + A^+) - e^{i\xi(e^{-i2\gamma}A^+ - A^-)} A^+] \\
&= \frac{2\sqrt{D_1 D_2}}{D_1 + D_2} \left[\frac{e^{-i2\gamma}A^+}{e^{-i2\gamma}A^+ - A^-} - ie^{-i2\gamma}A^{+2} \int_0^1 d\rho(1-\rho)e^{-ie^{-i2\gamma}A^{+2}\rho(1-\rho) + i\rho A^+ A^-} \right]. \tag{B3}
\end{aligned}$$

By performing a partial integration of the second term (so as to subtract the term linear in ρ of the integrand), we finally obtain

$$\begin{aligned}
I &= \frac{2\sqrt{D_1 D_2}}{D_1 + D_2} \left[\frac{1}{2} \left(e^{iA^+ A^-} - \frac{A^- + A^+ e^{-i2\gamma}}{A^- - A^+ e^{-i2\gamma}} \right) - \frac{i}{2} A^+ (A^+ e^{-i2\gamma} + A^-) \int_0^1 d\rho e^{-i[A^{+2} e^{-i2\gamma}\rho(1-\rho) - A^+ A^- \rho]} \right] \\
&= \frac{C}{2} \left[e^{-\frac{i}{2}(A^2 + \tilde{A}^2)} - i\frac{A}{\tilde{A}} + iA \int_{-i\tilde{A}}^A dA' e^{-\frac{i}{2}(\tilde{A}^2 + A'^2)} \right] \tag{B4}
\end{aligned}$$

with the following variables:

$$\begin{aligned}
\mathcal{A} &\equiv \frac{i}{\sqrt{2}} (A^+ e^{-i\gamma} + A^- e^{i\gamma}) \\
&= \sqrt{\frac{D_1 + D_2}{2D_1 D_2}} \left(A + A^* \frac{D_1 - D_2}{D_1 + D_2} \right), \tag{B5}
\end{aligned}$$

$$\tilde{\mathcal{A}} \equiv \frac{1}{\sqrt{2}} (A^+ e^{-i\gamma} - A^- e^{i\gamma}) = \sqrt{\frac{2}{D_1 + D_2}} A^* \tag{B6}$$

$$\mathcal{A}' \equiv -i\tilde{\mathcal{A}} + i\sqrt{2}A^+ e^{-i\gamma}\rho, \quad C = \sin(2\gamma) = \frac{2\sqrt{D_1 D_2}}{D_1 + D_2}. \tag{B7}$$

Finally, an integration by parts shows that I is identically given by

$$I = -C \frac{\mathcal{A}}{2} \int_{-i\tilde{\mathcal{A}}}^{\mathcal{A}} \frac{d\mathcal{A}'}{\mathcal{A}'^2} e^{-\frac{i}{2}(\tilde{\mathcal{A}}^2 - \mathcal{A}'^2)}: \tag{B8}$$

- (i) It is easily verified that Eq. (B8), with the identification (B5), is the solution of the differential equation (B2) with boundary condition $\mathcal{A}_{\text{in}} = -i\tilde{\mathcal{A}}$.
- (ii) If $D_1 = 1 = D_2$, as in the case of the emission amplitude discussed in Sec. II E, $C = 1$, $\mathcal{A} = A$, and $\tilde{\mathcal{A}} = A^*$. In particular, Eq. (B8) reduces to Eq. (2.47).
- (iii) \mathcal{A} and $\tilde{\mathcal{A}}$ are not complex conjugate for $D_1 \neq D_2$.

- (iv) The amplitude vanishes when the integration limits coincide, i.e., $\mathcal{A} = -i\tilde{\mathcal{A}}$, corresponding to $A^+ = A_2/\sqrt{D_1} + A_1/\sqrt{D_2} = 0$, or equivalently $\phi_A = -\gamma$. In the limit $D_1 = D_2$, such a nodal line corresponds

to the azimuthal direction $\phi_A = -\pi/4$, while γ becomes possibly small for $D_1 \ll D_2$, as depicted in Fig. 13.

-
- [1] G. 't Hooft, *Phys. Lett. B* **198**, 61 (1987).
 [2] I. J. Muzinich and M. Soldate, *Phys. Rev. D* **37**, 359 (1988).
 [3] D. Amati, M. Ciafaloni, and G. Veneziano, *Phys. Lett. B* **197**, 81 (1987).
 [4] D. J. Gross and P. F. Mende, *Phys. Lett. B* **197**, 129 (1987).
 [5] D. Amati, M. Ciafaloni, and G. Veneziano, *Int. J. Mod. Phys. A* **03**, 1615 (1988).
 [6] H. L. Verlinde and E. P. Verlinde, *Nucl. Phys.* **B371**, 246 (1992).
 [7] D. Amati, M. Ciafaloni, and G. Veneziano, *Nucl. Phys.* **B347**, 550 (1990).
 [8] D. Amati, M. Ciafaloni, and G. Veneziano, *Nucl. Phys.* **B403**, 707 (1993).
 [9] D. Amati, M. Ciafaloni, and G. Veneziano, *J. High Energy Phys.* 02 (2008) 049.
 [10] G. Marchesini and E. Onofri, *J. High Energy Phys.* 06 (2008) 104.
 [11] G. Veneziano and J. Wosiek, *J. High Energy Phys.* 09 (2008) 023.
 [12] G. Veneziano and J. Wosiek, *J. High Energy Phys.* 09 (2008) 024.
 [13] A. Gruzinov and G. Veneziano, *Classical Quantum Gravity* **33**, 125012 (2016).
 [14] G. Dvali, C. Gomez, R. Isermann, D. Lüst, and S. Stieberger, *Nucl. Phys.* **B893**, 187 (2015).
 [15] M. Ciafaloni, D. Colferai, and G. Veneziano, *Phys. Rev. Lett.* **115**, 171301 (2015).
 [16] A. Addazi, M. Bianchi, and G. Veneziano, [arXiv:1611.03643](https://arxiv.org/abs/1611.03643).
 [17] L. N. Lipatov, *Nucl. Phys.* **B365**, 614 (1991).
 [18] S. B. Giddings, D. J. Gross, and A. Maharana, *Phys. Rev. D* **77**, 046001 (2008).
 [19] M. Ciafaloni, D. Colferai, F. Coradeschi, and G. Veneziano, *Phys. Rev. D* **93**, 044052 (2016).
 [20] G. F. Giudice, R. Rattazzi, and J. D. Wells, *Nucl. Phys.* **B630**, 293 (2002).
 [21] V. S. Rychkov (private communication).
 [22] S. B. Giddings and V. S. Rychkov, *Phys. Rev. D* **70**, 104026 (2004).
 [23] H. Grigoryan and G. Veneziano (private communication).
 [24] S. W. Hawking, *Commun. Math. Phys.* **43**, 199 (1975).
 [25] S. W. Hawking, [arXiv:1509.01147](https://arxiv.org/abs/1509.01147).
 [26] M. Ciafaloni and D. Colferai, *J. High Energy Phys.* 10 (2014) 85.
 [27] X. O. Camanho, J. D. Edelstein, J. Maldacena, and A. Zhiboedov, *J. High Energy Phys.* 02 (2016) 020.
 [28] S. Weinberg, *Phys. Rev.* **140**, B516 (1965).
 [29] L. Lipatov, *Sov. Phys. JETP* **55**, 582 (1982).
 [30] M. Ciafaloni and D. Colferai, *J. High Energy Phys.* 11 (2008) 047.
 [31] M. Ciafaloni and D. Colferai, *J. High Energy Phys.* 12 (2009) 062.
 [32] M. Ciafaloni, D. Colferai, and G. Falcioni, *J. High Energy Phys.* 09 (2011) 044.
 [33] P. Aichelburg and R. Sexl, *Gen. Relativ. Gravit.* **2**, 303 (1971).
 [34] V. A. Abramovsky, V. N. Gribov, and O. V. Kancheli, *Yad. Fiz.* **18**, 595 (1973) [*Sov. J. Nucl. Phys.* **18**, 308 (1974)].